

1 General comments

2 The description of the SOM and the transition between nodes is good.

3 Please refer to figures more throughout the results section. I'd cite the figure number each
4 time you change which figure you are discussing. For example, on line 230 you mention
5 Figure 6, but then in the following line you are referring to Figure 5 but you do not give the
6 figure number. It would be easy here (and in other places) for the reader to be looking at the
7 wrong figure. The paragraph starting at line 277 is another instance where figures should be
8 referred to more frequently.

9 **Good suggestion. We have gone through the manuscript carefully and added citations to**
10 **figures whenever appropriate.**

11

12 Datasets and methods section – this section provides a good explanation of SOMs, including
13 what SOMs are and how you will apply them to temperature data, but there is no explanation
14 of how you analyse the other variables (i.e. create composites based on the SOM for
15 temperature data), or the use of principal component analysis. Please include this here.

16 **Thanks for pointing out this oversight. We have added more description about the other**
17 **methods we also used in the analyses, in addition to SOM, in the Method section.**

18

19 Consider adding analysis to show what portion of the trend in the warm Arctic-cold
20 Eurasia pattern is due to mean warming. What trend is removed from the 20CR data?
21 It seems an oversight to not consider mean warming when so many other variables are being
22 examined.

23 **Trend in wintertime surface air temperature anomalies for the 1854-2014 period for the 20CR**
24 **data was removed.**

25 **In this study, we mainly focused on the role of the interdecadal variability of SST anomalies**
26 **over northern oceans in trend in the warm Arctic-cold Eurasia pattern. In Conclusions and**
27 **Discussions section, we increased some discussions of the role of Arctic warming in the**
28 **trend.**

29 Specific comments

30 Lines 23-36 – Abstract nicely sums up the major findings of the paper.

31 **Thanks**

32 Line 53 – This line states that the warm Arctic-cold continents pattern has been observed on
33 an interannual timescale. Please state here whether the pattern has been strengthening linearly
34 over time, or whether it's a cyclical pattern, or something else.

35 **We have added a statement here about increasing trend in the occurrence of the warm**
36 **Arctic-cold continents pattern.**

37 Line 75 – What changes in the Gulf Stream are you referring to here?

38 **Changed the statement to "... the sea surface temperature anomalies over the Gulf Stream."**

39 Line 85 – "Using regression method" should probably read "using regression", or "using
40 linear regression" (if this is correct).

41 **Changed to 'using linear regression'**

42 Lines 90-98 – This first part of the Datasets and methods section seems to be replicating some
43 of what is said in section 2.2. I'd suggest starting the datasets and methods section with
44 section 2.1, and incorporating lines 90-98 into section 2.2.

45 **Removed the replications**

46 Line 94 – Should this say “41 winters”? Or are you only considering complete winters, i.e.
47 December 1979-February 2019 (thus excluding January and February 1979, and
48 December 2019)? Which months do you use for winter? I assume it’s DJF.
49 **Winter is defined by DJF and we only consider complete winters from December 1979**
50 **through February 2019. This is now clarified.**

51 Line 102 – What is the resolution of the ERA-Interim data?
52 **The resolution of the ERA-Interim was added.**

53 Lines 137-138 – What dataset are these lines referring to? Both ERA-Interim and
54 20CR? If both, which 40-year period do you use? I.e. do you subtract the 1979-2019 mean
55 from both datasets?
56 **These lines refer to ERA-Interim reanalysis. We subtract the 1979-2019 mean from**
57 **ERA-Interim.**

58 Line 150 – Do the SOM-explained trends mean something physically, i.e. are they the
59 fraction of the total trends that are explained by changes in circulation (or something else)?
60 **The SOM-explained trends are the fraction of the total trends that are explained by the**
61 **changes in circulations.**

62 Lines 161-162 – This sentence compares the “first node” in each group, however node
63 9 appears to be the second node in group one, and node 1 is the first node in group two.
64 **Changed**

65 Lines 164-165 – It is not clear from Figure 1 that the maximum anomalies are centered near
66 Svalbard. Please consider adding contour lines to the SOMs, or use a discrete color scale.
67 When you say maximum, are you referring to the greatest departure from zero (i.e. positive or
68 negative values)?
69 **Contour lines are added. Maximum refers to largest values of the anomalies**

70 Line 165 – This line states that nodes 3 and 7 are the second most frequently occurring of
71 their groups, but node 3 occurs most frequently. The comparison of pairs is good, but needs to
72 be worded more carefully. Maybe pick the most frequently occurring node in group 1 then
73 identify its pair.
74 **Good suggestion. Statements rephrased.**

75 Lines 171-172 – Why can’t this SOM consider temperature trends? I think this should say
76 “does not” not “cannot”.
77 **Changed to “does not”**

78 Lines 176-180 – Consider moving these lines to the methods section.
79 **We have added some description on composite method in the Method section, following**
80 **another reviewer’s comment.**

81 Line 193 – Please add figure reference.
82 **Referred more to figures whenever appropriate.**

83 Line 223 – Nice explanation of turbulent heat flux!
84 **Thanks**

85 Line 229 – Maybe refer back to Figures 2 and 3 if that is where this statement comes from.
86 **Made references back to the figures**

87 Lines 229-230 – Are you sure this is the correct order? I.e. over the Barents Sea in node 1, is
88 it possible that the sea ice melt causes a reduction in the albedo which results in an increased

89 turbulent heat flux?
90 We believe the cause-effect is correct based on previous studies (Blackport et al., 2019)
91 Line 231 – When you say “larger” do you mean larger spatially, or a greater magnitude
92 anomaly?
93 A greater magnitude anomaly. Clarified
94 Line 238 – “composted” should probably be “composited”.
95 Changed
96 Line 239 – What happens if you do the same lag analysis for sea ice concentration? I think it
97 is important to know that sea ice does not also peak before the day the nodes occur. Similarly,
98 what happens if you do this lag analysis on the geopotential height patterns?
99 It seems strange to say that circulation leads sea ice cover without mentioning the
100 geopotential height patterns.
101 The pattern of the composited anomalous 500-hPa geopotential height, turbulent heat flux,
102 and sea ice concentration 2 days prior to the day when the nodes occur (not shown) is similar
103 to the simultaneous pattern in Figures 2, 5, and 6.
104 Lines 250-251 – How does this differ to the other nodes? I assume they only exhibit
105 interannual variability.
106 The main difference is the decadal variability.
107 Line 255 – I think this should refer to Table 3 (not Table 2).
108 Changed
109 Line 261 – Figure 8 does not appear to cover a large enough region to determine whether
110 there are positive trends over southern Europe. This might need re-wording.
111 Rewording done
112 Line 262 – Maybe point out that negative trends are mostly not significant.
113 Done
114 Line 267 – Arctic–cold should be Arctic-cold
115 Changed
116 Line 281 – Refer to figure number (Figure 11).
117 Added reference to Figure 11
118 Lines 282-285 – Which node are you referring to? I assume node 1 but this should be clear.
119 Added reference to node 1.
120 Lines 284-285 – Are you determining the direction of propagation from Figure 11 or Figure
121 12? From the text it sounds like you are only referring to Figure 11, but I am not sure how
122 you are determining that the Rossby wave moves southeastwards to the Eurasian continent
123 from this figure. Please explain and give figure number.
124 The direction of wave activity flux points to the Eurasian continent (Figure 12). A reference
125 to Figure 12 is added.
126 Lines 285-286 – What figure(s) support the claim that “large SST anomalies over the
127 Nordic Ocean augment the wave signal through local air-sea interaction”? This statement
128 needs more support and/or more of a description on how you came to this conclusion.
129 Added more descriptions with reference to figures
130 Line 290 – Figure number?
131 Added
132 Line 302 – Does “these results” refer to the results in Figures 10-12, or to the results you just

133 mentioned in lines 299-302? If you're referring to Figures 10-12, please state this.
134 **Reference to Figures 10-12 are added**
135 Line 308 – Which figure are you referring to here? If this comparison is not shown, write
136 “(not shown)”.
137 **“(not shown)” was added.**
138 Line 321 – Where it states that the magnitude is smaller for the 20 CR data, could this be
139 because the 20 CR data are detrended and the ERA-Interim data are not?
140 **Added detrending of the 20CR as a potential explanation**
141 Lines 321-322 – This sentence says “frequencies of all the nodes (Figure 14)”, but Figure 14
142 only shows data for nodes 1, 4, 6, and 9 – please rectify.
143 **Clarified**
144 Line 322 – Please refer to the corresponding figure that shows node occurrence for
145 ERA-Interim.
146 **Reference to corresponding figures added**
147 Line 325 – The occurrence frequencies at the end of the time series in node 1, Figure 7,
148 appear to be slightly greater than those for node 1 in Figure 14. Could this indicate that mean
149 warming amplifies these trends?
150 **Global warming may be a reason**
151 Lines 335-336 – If these results are not shown, please state this.
152 **Stated**
153 Lines 343-344 – Why isn't the central North Pacific Ocean SST index shown in Figure
154 15 since it is significantly correlated with EOF modes 1 and 2?
155 **The central North Pacific Ocean SST index is added in Figure 15**
156 Line 347 – And the PDO?
157 **Added**
158 Lines 386-387 – Which figures are you referring to here?
159 **References to corresponding figure added**
160 Lines 388-389 – How does this atmospheric process suggest that the relationship between a
161 warmer Arctic and East Asian cold spells are not as strong? If the atmospheric patterns
162 described by your SOMs show changes in circulation patterns lead to increases in Arctic
163 temperatures and decreases in Eurasian temperatures, then there appears to be a strong link.
164 Or are you saying that temperature increases in the Arctic are not the driver of temperature
165 decreases in Eurasia?
166 **Temperature increases in the Arctic are not the driver of temperature decreases in Eurasia.**
167
168 **Figures**
169 In general - Please add the following to the figure captions: - What years the figure covers (if
170 not shown). E.g. Figure 1 - Whether the data have been detrended or not -
171 Dataset used - Consider making figures more consistent, for example, Figure 10 has the
172 Pacific Ocean in the center, whereas Figure 12 has the Atlantic in the center. It would be
173 easier to compare these figures if they both had the same east/west bounds.
174 **Years and data were added in figure captions. Figure 10 has changed.**
175 Figure 1 - Please consider adding contour lines to the SOM, or use a discrete color scale so it
176 is clearer where the maximum/minimum values are on these plots. – Please mention years and

177 dataset in the caption.

178 **Figure 1 has been changed into contour lines.**

179 Figure 2 - Please reconsider the use of a rainbow color scale. Reds and greens can look
180 identical to color blind people. - It appears that the stippling/hatching is plotted on top of the
181 contour lines. The plot might be easier to read if the contour lines were on top of the
182 stippling/hatching. - The caption states that this is the “corresponding 500-hPa
183 geopotential height anomalies”, but you do not mention that it corresponds to Figure
184 1. - The caption states that stippled areas are significant, but what about the hatched areas? I
185 assume they are also significant. - Please mention what contour lines show in caption. -
186 Maybe consider rotating the nodes so they match Figure 1 better, i.e. put Russia at the bottom
187 of the subplots. Alternatively, adding an outline of the region in Figure 1 to the plots like
188 Figure 2 would be helpful.

189 **Rainbow color scale is now used. An outline of the region in Figure 1 is added. We used
190 stippled, not hatched in Figure 2.**

191 Figure 3 - It would be useful to show the contour lines (from Figure 2) on this plot as well
192 (without stippling) so we can see exactly how the contour lines and wind anomalies line up. -
193 What does the gray shading mean?

194 **Adding contour lines made it harder to see vectors. We replaced stippling by shading to denote
195 the above 95% confidence level.**

196 Figure 6 - Node numbers are missing from Figure 6. Please add them.

197 **Added**

198 Figure 7 - Consider adding trend lines and p-values to each subplot (and other similar
199 figures).

200 **Added**

201 Figures 10, 11, and 12 - Consider arranging these plots the same, i.e. all 2x2 or 1x4 for easier
202 comparison between the figures.

203 **Rearranged**

204 Figure 14 - Can the results from Figure 7 be overlaid on Figure 14? Maybe with gray dashed
205 outlines. This would make it clearer to see the similarities/differences between the results.

206 **The time series in Figure 7 is added in Figure 14**

207 Figure 15 - Consider putting r and p values on subplots b and d. Or in caption.

208 **R and P values are added in the caption**

209

210

211

212

213

214

215 **Revisiting the trend in the occurrences of the “warm Arctic-cold Eurasian continent”**

216 **temperature pattern**

217 Lejiang Yu^{1,2*}, Shiyuan Zhong³, Cuijuan Sui⁴, and Bo Sun¹

218 1MNR Key Laboratory for Polar Science, Polar Research Institute of China, Shanghai, China

219 2 Southern Marine Science and Engineering Guangdong Laboratory (Zhuhai), Zhuhai, Guangdong,

220 China

221 3Department of Geography, Environment and Spatial Sciences, Michigan State University, East

222 Lansing, MI, USA

223 4 National Marine Environmental Forecasting Center, Beijing, China

224

225 *Corresponding Author’s address

226 Dr. Lejiang Yu

227 MNR Key Laboratory for Polar Science, Polar Research Institute of China

228 451 Jinqiao Rd. Shanghai, 200136

229 Phone: 86-21-58712034,

230 Email: yulejiang@sina.com.cn

231

232

233

234

235

236

237 **Abstract.** The recent increasing trend of “warm Arctic, cold continents” has attracted much attention,
238 but it remains debatable as to what forces are behind this phenomenon. Here, we revisited
239 surface-temperature variability over the Arctic and Eurasian continent by applying the
240 Self-Organizing-Map (SOM) technique to gridded daily surface temperature data. Nearly 40% of the
241 surface temperature trends are explained by the nine SOM patterns that depict the switch to the current
242 warm Arctic-cold Eurasia pattern at the beginning of this century from the reversed pattern that
243 dominated the 1980s and the 90s. Further, no cause-effect relationship is found between the Arctic
244 sea-ice loss and the cold spells in high-mid latitude Eurasian continent suggested by earlier studies.
245 Instead, the increasing trend in warm Arctic-cold Eurasia pattern appears to be related to the anomalous
246 atmospheric circulations associated with two Rossby wavetrains triggered by rising sea surface
247 temperature (SST) over the central North Pacific and the North Atlantic Oceans. On interdecadal
248 timescale, the recent increase in the occurrences of the warm Arctic-cold Eurasia pattern is a fragment
249 of the interdecadal variability of SST over the Atlantic Ocean as represented by the Atlantic
250 Multidecadal Oscillations (AMO), and over the central Pacific Ocean.

251

252 **Key words:** Warm Arctic-cold Eurasian continent, Arctic Sea ice, the Kara-Barents Sea, the
253 Self-Organizing-Map (SOM), the Pacific Decadal Oscillation (PDO), the Atlantic Multidecadal
254 Oscillation (AMO)

255

256

257

258

259 **1 Introduction**

260 In recent decades, winter season temperature in the Arctic has been rising at a rate faster than the
261 warming experienced in any other regions of the world (Stroeve et al., 2007; Screen and Simmonds,
262 2010; Stroeve, 2012). In contrast, there has been an increasing trend in colder than normal winters
263 over the northern mid-latitude continents (Mori et al., 2014; [Cohen et al., 2014; 2018](#)). This pattern of
264 opposite winter temperature trend between the Arctic and high-mid latitude continents, referred to as
265 the warm Arctic-cold continents pattern (Overland et al., 2011; Cohen et al., 2014; Walsh, 2014), has
266 ~~also been observed on the interannual timescale~~[received considerable interest in the scientific](#)
267 [community especially with regard to dynamical and physical mechanisms for the development of the](#)
268 [phenomenon](#) (Mori et al., 2014; ~~Kug et al., 2015~~)~~The question as to what processes are responsible for~~
269 ~~the opposite change of winter air temperature between the Arctic and mid latitudes remain open~~
270 (~~Vihma, 2014; Barnes and Screen, 2015; Kug et al., 2015; Overland et al., 2015; Chen et al., 2018~~).

271 [Using observational analyses or coupled ocean-atmosphere modeling](#), ~~A~~ number of studies have
272 attributed the recent warm Arctic-cold continents pattern to the Arctic sea ice loss [in boreal winter](#)
273 (Inoue et al., 2012; Tang et al., 2013; Mori et al., 2014; Kug et al., 2015; Cohen et al., 2018; Mori et al.,
274 2019). Sea ice variability in different parts of the Arctic Ocean has been linked to climate variability in
275 different parts of the world. Specifically, sea ice loss in the Barents and Kara Seas has been linked to
276 cold winters over East Asia ~~(add a reference~~ [Kim et al., 2014; Mori et al., 2014; Kug et al., 2015;](#)
277 [Overland et al., 2015](#)) [and in central Eurasia \(Mori et al., 2014\)](#), while a similar connection has been
278 found between cold winters in North America and sea ice retreat in the East Siberian and Chukchi Seas
279 (Kug et al., 2015). A most recent study (Matsumura and Kosaka, 2019) attributed the warm Arctic-cold
280 continents pattern to the combined effect of Arctic sea ice loss and the atmospheric teleconnection

281 induced by tropical Atlantic sea-surface temperature (SST) anomalies. ~~Some recent studies have~~
282 ~~suggested that the mid-latitude atmospheric circulation anomalies play a role in the formation of the~~
283 ~~warm Arctic-cold continents pattern (Luo et al., 2016; Peings et al., 2019).~~

284 Other studies, however, found no cause-and-effect relationship between Arctic sea ice loss and
285 mid-latitude climate anomalies (Blackport et al., 2019; Fyfe, 2019). Numerical modeling studies using
286 coupled ocean and atmospheric models simulated no cold mid-latitude winters when the models were
287 forced with reduced Arctic sea ice cover (McCusker et al., 2016; Sun et al., 2016; Koenig et al., 2019;
288 Blackport et al., 2019; Fyfe, 2019). ~~Instead, The results from~~ these studies pointed to internal
289 atmospheric variability as the likely cause for cold winters in mid-latitudes. Some studies have also
290 suggested that on the interannual timescale mid-latitude atmospheric circulation anomalies triggered by
291 the Pacific and Atlantic SST oscillations may explain both the Arctic sea ice loss and the cooling of the
292 high-mid latitudes (Lee et al., 2011; [Luo et al., 2016](#); [Peings et al., 2019](#); Matsumura and Kosaka, 2019;
293 Clark and Lee, 2019). The [sea surface temperature anomalies over the](#) Gulf Stream ~~have~~ ~~has~~ also been
294 linked to the Barents Sea ice loss and Eurasian cooling (Sato et al., 2014).

295 Despite the recent attention given to the warm Arctic-cold continents pattern, it remains debatable
296 as to ~~what the roles of various dynamical and physical~~ processes ~~play may be responsible in the~~
297 ~~formation of~~ ~~for~~ this phenomenon. In this study, we revisit surface temperature variability over the
298 Arctic and Eurasia continent (40-90°N, 20-130°E), where the warm Arctic-cold continents pattern is a
299 prominent feature (Cohen et al., 2014; Mori et al., 2014), by applying the Self-Organizing-Map (SOM)
300 technique to daily surface temperature over the recent four decades. We will show that while the warm
301 Arctic-cold Eurasian continent pattern has dominated the recent two decades, its opposite pattern, cold
302 Arctic-warm Eurasia continent, appeared frequently in the 1980s and the 90s. Using century-long data,

303 we will further show that the warm Arctic-cold Eurasian continent pattern is an intrinsic climate mode
304 and the recent increasing trend in its occurrence is a reflection of an interdecadal variability of the
305 pattern. Using [linear regression](#)~~-method~~, we explain the reason for the recent increasing occurrences of
306 the warm Arctic-cold continents pattern. We also assess the role of the SST anomalies over the North
307 Pacific and Atlantic Oceans in the variability of the warm Arctic-cold Eurasia pattern on the
308 interdecadal time scale.

309 2 Datasets and methods

~~310 From the perspective of nonlinear dynamic, a region's climate has its intrinsic modes of variability, but
311 the frequency of occurrence of these internal modes can be modulated by remote forces external to the
312 region (Palmer, 1999; Hoskins and Woollings, 2015; Shepherd, 2016). In this study we will first obtain
313 the main modes of variability of wintertime surface temperature in a region (40-90 N, 20-130 E) by
314 applying the SOM method (Kohonen, 2001) to daily surface temperature data for the 40 winters in the
315 1979-2019 period. The use of daily data over four decades allows for capturing the variability across
316 two time scales (synoptic and decadal). We will then determine, through regression and composite
317 analyses, the relationships of these modes of climate variability of surface air temperature to known
318 climate variability modes at corresponding time scales.—~~

319 2.1 Datasets

320 Daily surface air temperature and other climate variables used in the current analyses, including
321 500 hPa geopotential height, 800-hPa wind and mean sea level pressure, all come from the [European
322 Centre for Medium-Range Weather Forecasts Re-Analysis \(ERA\)](#), the interim version (ERA-Interim;
323 Dee et al., 2011) [with a horizontal resolution of approximately 79 km \(T255\) and 60 vertical levels in
324 the atmosphere](#). Compared to the earlier versions of ERA (e.g., ERA-40, Uppala et al., 2005) and other

325 global re-analysis products (e.g. the NCEP reanalysis, Kalnay et al., 1996), ERA-Interim has been
326 found to be more accurate in portraying the Arctic warming trend (Dee et al., 2011; Screen and
327 Simmonds, 2011) despite its known warm and moist bias in the surface layer (Jakobson et al., 2012).

328 Daily sea ice data are obtained from the U.S. National Snow and Ice data Center
329 (ftp://sidacs.colorado.edu/DATASETS/nsidc0051_gsfc_nasateam_seaice/final-gsfc/north/daily).

330 Gridded monthly SST data used in the current analysis are obtained from the U.S. National Oceanic
331 and Atmospheric Administration (NOAA) data archives
332 (<ftp://ftp.cdc.noaa.gov/Datasets/noaa.oisst.v2.highres/>) (Reynolds et al. 2007).

333 The results obtained from the data within the recent four decades are put into the context of the
334 variability over longer time scales using data from the Twentieth Century Reanalysis project, version
335 2Ce (20CR) that spans more than a century from 1851 through 2015 (Compo et al., 2011). The 20CR
336 reanalysis data, which has a horizontal resolution of 2 °latitude by 2 °longitude and temporal resolution
337 of 6 hours, ~~Through the assimilation of surface observational pressure data, the 20CR reanalysis~~ was
338 produced by ~~the~~ model ~~whose driven at the~~ lower boundary ~~by condition is derived from observed~~
339 monthly SST and sea ice conditions and with data assimilation of surface pressure observations.
340 ~~Various~~ Several indices used to describe known modes of climate variability ~~are obtained from~~
341 ~~NOAA's Climate prediction Center (CPC) (<https://www.esrl.noaa.gov/psd/data/climateindices/list/>),~~
342 ~~which~~ include Arctic oscillation (AO), Northern Atlantic Oscillation (NAO), Atlantic Multidecadal
343 Oscillation (AMO) (Enfield et al., 2001) and PDO (Mantua et al., 1997) ~~indices, are obtained from~~
344 NOAA's Climate prediction Center (CPC) (<https://www.esrl.noaa.gov/psd/data/climateindices/list/>).

345 2.2 Methods

346 From the perspective of nonlinear dynamic, a region's climate has its intrinsic modes of variability,

347 but the frequency of occurrence of these internal modes can be modulated by remote forces external to
348 the region (Palmer, 1999; Hoskins and Woollings, 2015; Shepherd, 2016). In this study we will first
349 obtain the main modes of variability of wintertime surface temperature in a region (40-90°N, 20-130°E)
350 by applying the SOM method (Kohonen, 2001) to daily surface temperature data for the 40 winters
351 (December, January, -February) in the 1979-2019 period from December 1979 through February 2019.
352 The use of daily data over four decades allows for capturing the variability across two time scales
353 (synoptic and decadal). ~~The 40-year, daily surface temperature over the study region (40-90°N,~~
354 ~~20-130°E) is decomposed using the SOM method.~~ SOM is a clustering method based on neural
355 network that can transform multi-dimensional data into a two-dimensional array without supervised
356 learning. The array includes a series of nodes arranged by a Sammon map (Sammon, 1969). Each node
357 in the array has a vector that can represent a spatial pattern of the input data. The distance of any two
358 nodes in the Sammon map represents the level of similarity between the spatial patterns of the two
359 nodes. Because SOM has fewer limitations than most other commonly used clustering methods, (e.g.,
360 orthogonality required by the empirical orthogonal function or EOF method), the SOM method can
361 describe better the main variability patterns of the input data (Reusch et al., 2005).

362 SOM method has been used in atmospheric research at mid and high latitudes of the northern
363 hemisphere (Skific et al., 2009; Johnson and Feldstein, 2010; Horton et al., 2015; Loikith and Broccoli,
364 2015; Vihma et al., 2019). For example, Johnson and Feldstein (2010) used SOM to identify~~ied the~~
365 spatial patterns of ~~the~~ daily wintertime North Pacific sea level pressure and related ~~the~~ the variability of the
366 occurrences of those patterns to some large-scale circulation indices. Loikith and Broccoli (2015)
367 compared observed and model-simulated circulation patterns across the North American domain using
368 an approaching involving SOM. The SOM method was also used to detect circulation pattern trends in

369 a subset of North America during two [different](#) periods (Horton et al., 2015).
370 In this study, the SOM method is applied to [ERA-Interim](#) wintertime daily temperature anomalies [from](#)
371 [December 1979 through February 2019. The anomalies are calculated](#)~~obtained~~ by subtracting 40-year
372 averaged daily temperature from the original daily temperature at each grid point. Prior to SOM
373 analysis, it is necessary to determine how many SOM nodes are needed to best capture the variability
374 in the data. According to previous studies (Lee and Feldstein, 2013; Gibson et al., 2017; Schudeboom
375 et al., 2018), the rule for determining the number of SOM nodes is that the number should be
376 sufficiently large to capture the variability of the data analyzed, but not too large to introduce
377 unimportant details. Table 1 shows the averaged spatial correlation between all daily surface air
378 temperature [anomalies](#) and their matching nodes. ~~There is an increase in~~ [The spatial](#) correlation
379 coefficients [increase](#) from 0.26 for a 3×1 grid to 0.51 for a 4×4 grid, but the gain from a 3×3 grid to a
380 4×4 grid is relatively small. Hence, a 3×3 grid seems to meet the above-mentioned rule and will be
381 utilized in this study.

382 The contribution of each SOM node to the trend in wintertime surface temperature [anomalies](#) is
383 calculated by the product of each node pattern and its frequency trend normalized by the total number
384 [\(90\)](#) of wintertime days ~~(90,~~ Lee and Feldstein, 2013). The sum of the contributions from all nodes
385 denotes the SOM-explained trends. Residual trends are equal to the subtraction of SOM-explained
386 trends from the total trends. [The anomalous atmospheric circulation pattern corresponding to each of](#)
387 [the SOM pattern is obtained by composite analysis that computes a composite mean of an atmospheric](#)
388 [circulation field \(e.g., 500 hPa height\) over all occurrences of that SOM node. Regression analysis is](#)
389 [also performed where atmospheric circulation variables are regressed onto the time series of the](#)
390 [occurrence of a SOM node to further elucidate the relationship between the variability of atmospheric](#)

391 [circulations and surface temperatures](#). The statistical significance [of composite and regression analyses](#)
392 in this study is tested by using the Student's t test.

393 **3 Results**

394 3.1 Surface temperature variability

395 The majority of the 9 SOM nodes depict a dipole pattern characterized by opposite changes in
396 [surface temperatures](#) between the Arctic Ocean and the Eurasian continent, although the sign switch
397 does not always occur at the continent-ocean boundary (Figure 1). The [differences in the](#) position of the
398 boundary between the warm and cold anomalies [reflects](#) the transition between the cold Arctic-warm
399 Eurasia pattern (denoted, in descent order of the occurrence frequency, by nodes 3, 9, 6), to the warm
400 Arctic-cold Eurasia pattern (depicted, in descent order of the occurrence frequency, by nodes 1, 7, 4).

401 The spatial patterns represented by the first group of nodes (~~3, 9, 6~~) are almost mirror images of the
402 patterns denoted by the corresponding nodes in the second group (~~1, 7, 4~~). For example, the ~~first-second~~
403 node in group 1 (node 9, 15.4%) and [the first node](#) in group 2 (node 1, 17.1%) show a mirror image
404 pattern with cold (warm) anomalies in the Arctic Ocean extending into northern Eurasia and warm
405 (cold) anomalies in the rest of the Eurasia continent in the study domain. In both cases, the region of
406 maximum ~~anomalies-magnitude anomalies~~ is centered near Svalbard, Norway. The second ~~most~~
407 ~~frequent-patternpair~~, denoted by node 3 (17.2%) and 7 (13.7%) ~~in the two groups, respectively~~, has the
408 boundary of separation moved northward from northern Eurasia continent toward the shore of the
409 Arctic Ocean. While the maximum anomaly in the Arctic Ocean remains close to Svalbard, maximum
410 values over the continent are found in central Russia. Nodes 4-6 display a noticeable transition from
411 node 1 to node 7 and from node 3 to node 9, respectively. Although nodes 2 and 8 show an
412 approximate monopole spatial pattern, they also represent a transition between nodes 1 and 3, and

413 between nodes 7 and 9, respectively. Above SOM analysis ~~cannot~~does not consider the trend in surface
414 air temperature. The result is similar ~~while when removing~~ the trend is removed (~~Not-not~~ shown).

415 The temporal variability on this time scale is typically related to synoptic processes and hence the
416 questions are what synoptic patterns are responsible for the occurrence of the spatial patterns depicted
417 by each of the 9 SOM nodes and how these patterns are related to those of the Arctic sea ice anomalies?

418 These questions can be answered by using the composite method. Specifically, for each SOM node,
419 composite maps are made respectively for the anomalous 500-hPa geopotential height, mean sea level
420 pressure, 850-hPa wind, downward longwave radiation, surface turbulent heat flux, and sea ice
421 concentration over all the days when the spatial variability of the surface temperature anomalies is best
422 matched by the spatial pattern of that node.

423 3.2 Large-scale circulation patterns

424 For all SOM nodes, the spatial pattern of the composited 500 hPa-geopotential height anomalies
425 (Figure 2) is similar to that of mean sea level pressure anomalies (~~Not-not~~ shown), indicating an
426 approximately barotropic structure. For nodes 1, 4 and 7, the 500-hPa height anomalies show a dipole
427 structure of positive values over Siberia and negative values to its south over the Eurasian continent.

428 Anomalous southwesterly winds on the western side of the anticyclone over Siberia transport warm
429 and moist air from northern Europe and the North Atlantic Ocean into the Atlantic sector of the Arctic
430 Ocean (Figure 3), providing a plausible explanation of the warm surface temperature anomalies in the
431 region (Figure 1). On the eastern side of the anticyclone, anomalous northwesterly winds bring cold
432 and dry air from the Arctic Ocean into Eurasia continent, which is consistent with the negative surface
433 temperature anomalies there. The opposite occurs for nodes 3, 6 and 9. A similar explanation involving
434 anomalous pressure and wind fields can be applied to other nodes. The dipole structure that dominates

435 the anomalous 500-hPa height fields over the North Atlantic Ocean for most nodes resembles the
436 spatial pattern of the NAO (Figure 2). In addition, the patterns for ~~several~~ a few nodes, such as nodes 4
437 and 7, have some resemblance to the spatial pattern of the AO over larger geographical region. The
438 possible connection to NAO and AO is further investigated by averaging the daily index values of
439 NAO or AO over all occurrence days for each node. The results (Table 2) show that nodes 1, 2, 3 (5, 8,
440 9) correspond to a significant positive (negative) phase of the NAO index characterized by negative
441 (positive) height anomalies over Iceland and positive (negative) values over the central North Atlantic
442 Ocean. Association is also found between nodes 1, 2, 3, and 6 (5, 7, 8, and 9) and the positive (negative)
443 phases of the AO index.

444 3.3 Downward radiative fluxes

445 Besides the anomalous circulation patterns, anomalous surface radiative fluxes may also play a role in
446 shaping the spatial pattern of surface temperature variability. In fact, the spatial pattern of the mean
447 anomalous daily downward longwave radiation for an individual node (Figure 4) is in good agreement
448 with the spatial pattern of the surface temperature anomalies of that node. In other words, increased
449 downward longwave radiation is associated with positive surface temperature anomalies, and vice
450 versa. As expected from previous studies (e.g., Sedlar et al. 2011), there is a significant positive
451 correlation between downward longwave radiative fluxes and the anomalous total column water vapor
452 and mid-level cloud cover (not shown). The correlation to low- and high-level cloud cover is, however,
453 not significant (~~Not~~ not shown). Most of the water vapor in both the Arctic and Eurasia is derived from
454 the North Atlantic Ocean, but the water vapor is transported into the Arctic by southwesterly flows and
455 into Eurasia by northwesterly winds. The anomalous shortwave radiation corresponding to each node
456 (not shown) is an order of magnitude smaller than that of the longwave radiation anomalies and has a spatial

457 pattern opposite to that of the mid-level cloud cover and the longwave radiation anomalies.

458 3.4 Sea ice

459 The analyses presented above attempt to explain the spatial pattern of surface temperature
460 variability for each node from the perspective of anomalous heat advection and surface radiative fluxes.

461 As mentioned earlier, there has been a debate in the literature about the role played by the sea ice
462 anomalies in the Barents and Kara Seas in the development of the warm Arctic-cold Eurasia pattern.

463 Here, we examine the anomalous turbulent heat flux (Figure 5) and sea ice concentration (Figure 6) for
464 each node. Turbulent heat flux is considered positive when it is directed from the atmosphere

465 downward to the ocean or land surfaces. Thus, a positive anomaly indicates either an increase in the
466 atmosphere-to-surface heat transfer or a decrease in the heat transfer from the surface to the atmosphere.

467 The magnitude of anomalous turbulent heat flux is found to be comparable to that of anomalous
468 downward longwave radiation (Figure 4). For all nodes, the heat flux anomalies are larger over ocean

469 than over land [\(Figure 5\)](#). For node 1, positive turbulent heat flux anomalies occur mainly over the
470 Barents Sea, the western and central North Atlantic Ocean and the eastern North Pacific Ocean,

471 indicating an increase in heat transport from the air to the ocean due possibly to an increase in vertical
472 temperature gradient caused by warm air advection associated with anomalous circulation [\(Figures 2](#)

473 [and 3\)](#). The downward heat transfer results in sea ice melt in the Greenland Sea and the Barents Sea
474 (Figure 6). For node 4, the anomalous southerly winds over the Nordic Sea produce larger positive

475 turbulent heat flux anomalies [\(Figure 5\)](#). For node 7, the anticyclone is located more northwards, which
476 generates opposite anomalous winds between the Nordic and northern Barents Seas and the southern

477 Barents Sea and thus opposite turbulent heat flux anomalies that are consistent with the opposite sea ice
478 concentration anomalies in the two regions [\(Figure 5\)](#). For nodes 3, 6, and 9, the anomalous cold air

479 from the central Arctic Ocean flows into warm water in the Nordic and Barents Seas, producing
480 negative turbulent heat flux anomalies and positive sea ice concentration anomalies ([Figures 5 and 6](#)).
481 Sorokina et al. (2016) noted that turbulent heat flux usually peaks 2 days before changes in surface
482 temperature pattern occur. The pattern of the composited anomalous [500-hPa geopotential height](#),
483 turbulent heat flux [and sea ice concentration](#) 2 days prior to the day when the nodes occur (not shown)
484 is similar to the current-day pattern in [Figures 2, 65, and 6](#). Our results support the conclusion of
485 Sorokina et al. (2016) and Blackport et al. (2019) that the anomalous atmospheric circulations lead to
486 the anomalous sea ice concentration in the Barents Sea.

487 [3.5 Contributions of SOM nodes to the trends in wintertime surface temperature](#)

488 The results above suggest that both the surface temperature anomaly patterns over the Arctic Ocean
489 and Eurasian continent and the sea ice concentration anomalies in the Nordic and Barents Seas can be
490 explained largely by changes in atmospheric circulations and the associated vertical and horizontal heat
491 and moisture transfer by mean and turbulent flows. Next, we assess the [trends of wintertime surface](#)
492 [temperature and the](#) contributions of these [SOM](#) nodes to the ~~trends in wintertime surface temperature~~.

493 We first examine the time series of the accumulated number of days for each node in each winter
494 for the 1979-2019 period (Figure 7). The time series for nodes 1, 4, 6, and 9 exhibit variability on
495 interannual as well as decadal time scales. The occurrence frequency is noticeably larger after 2003
496 than prior to 2003 for nodes 1 and 4, and vice versa for nodes 6 and 9, and the difference between the
497 two periods is significant at 95% confidence level. Given the spatial patterns of these four nodes
498 (Figure 1), this indicates that the warm Arctic-cold Eurasia pattern occurred more frequently after 2003.
499 A linear trend analysis of the time series for each node (Table [23](#)) reveals significant positive trends in
500 occurrence frequency for nodes 1 and 4 and significant negative trends for nodes 6 and 9, which agree

501 | with the result from a previous study (Clark and Lee, 2019; [Overland et al., 2015](#)) that suggested an
502 | increasing trend of the warm Arctic and cold Eurasia pattern.

503 | These trends in the occurrence frequency of the SOM nodes contribute to the trends in the total
504 | wintertime (DJF) surface temperature anomalies (Figure 8, top panel) that have significant positive
505 | trends over the Arctic Ocean and in regions of Northern and ~~Southern~~-Eastern Europe and negative,
506 | [mostly insignificant](#) trends in Central Siberia. The contribution, however, varies from node to node
507 | (Figure 9). Node 1 has the largest domain-averaged contribution of 18.7%, followed by its mirror node
508 | (node 9) at 10.1%. Nodes 4 and 6 account for 2.8% and 4.3% of the total trend, respectively. None of
509 | the remaining nodes explain more than 2%. All nodes together explain 39.5% of the total trend in
510 | wintertime surface air temperature. The spatial pattern of the SOM-explained trends (Figure 8, middle
511 | panel) is similar to the warm Arctic–cold continent pattern, whereas the residual trend resembles more
512 | the total trend (Figure 8 bottom panel).

513 | 3.6 Mechanisms

514 | The results presented above indicate that the SOM patterns explain nearly 40% of the trend in
515 | wintertime surface air temperature anomalies and majority of the contributions (35 out of 40%) come
516 | from the two pairs of the nodes (nodes 1, 9, and 4, 6). –The analyses hereafter will focus on these four
517 | nodes. Below we assess the atmospheric and oceanic conditions associated with the occurrences of the
518 | four nodes via regression analysis. Specifically, the anomalous seasonal SST and atmospheric
519 | circulation variables are regressed onto the normalized time series of the number of days when each of
520 | the four nodes occurs (Figures 10, 11, and 12).

521 | For node 1, the SST regression pattern in the Pacific Ocean shows significant positive anomalies
522 | over the tropical western Pacific Ocean and central North Pacific Ocean ([Figure 10](#)). The positive SST

523 anomalies also occur over most of the North Atlantic. Negative SST anomalies occur over the central
524 tropical Pacific Ocean, though they are not significant at 95% confidence level. The SST regression
525 pattern is reversed for node 9. The direction of wave activity flux indicates the direction of group speed
526 of stationary planetary wave. Here we calculate the wave activity flux defined by Takaya and
527 Nakamura (2001), which considers the influence of mid-latitude zonal wind (Figure 12). For node 1,
528 ~~The~~ the corresponding anomalous 500-hPa height regression (Figure 11) shows two Rossby wavetrains:
529 one is excited over the central Pacific Ocean and propagates northeastwards into North America and
530 North Atlantic Ocean, and the other, which displays ~~a~~ the stronger signal, originates from central North
531 Atlantic and propagates northeastwards to the Arctic Ocean and southeastwards to the Eurasian
532 continent ~~and the western Pacific Ocean (Figure 11 and 12). The large SST anomalies over the Nordic~~
533 ~~Ocean augment the wave signal through local air sea interaction. The wave activity flux and~~
534 ~~streamfunction exhibit well the horizontal propagating direction of the planetary wave.~~ For node 9, the
535 corresponding anomalous 500-hPa height and streamfunction show an opposite pattern, but the wave
536 activity flux is similar to that of node 1.

537 For node 4, the SST anomalies over the tropical Pacific Ocean appear to be in a La Niña state,
538 which shows stronger negative SST anomalies over the eastern tropical Pacific Ocean than those for
539 node 1 (Figure 10). The positive SST anomalies over the North Pacific shift more northwards relative
540 to that of node 1. The positive SST anomalies over the North Atlantic are weaker than those for node 1.
541 The corresponding wavetrain over the Pacific Ocean is stronger than that over the Atlantic Ocean
542 (Figure 11), which ~~is~~ seen also be observed in the pattern of wave activity and streamfunction (Figure
543 12). The corresponding pattern for node 6 is nearly reversed, but there are some noticeable differences
544 in the amplitude of the wavetrain and SST anomalies. For example, the magnitude of the anomalous

545 SST and the 500-hPa height over the central North Pacific is larger for node 6 than that for node 4.

546 Besides the above-mentioned variables, similar regression analysis is also performed for the
547 anomalous 850-hPa wind field and anomalous downward longwave radiation (~~Not-not~~ shown). Their
548 regression patterns, which are similar to those in Figures 3 and 4, explain well the decadal variability of
549 the number of days for nodes 1, 4, 6, and 9. Together, these results [in Figures 10-12](#) indicate that the
550 decadal variability of the occurrence frequency of the four nodes in recent decades is related to two
551 wavetrains induced by SST anomalies over the central North Pacific Ocean and the North Atlantic
552 Ocean ([Figures 10 and 11](#)). The aforementioned SST regression patterns over the Atlantic and Pacific
553 Oceans also show features of the AMO and PDO (Figure 10). Since both the AMO and PDO exhibited
554 a phase change in the late 1990s (Yu et al., 2017), the question is whether a similar change in the SOM
555 frequency also appear in the late 1990s. A comparison of the averaged frequency before and after 1998
556 shows a significant drop in frequency for nodes 6 and 9 and an increase in frequency for node 1 (~~not~~
557 [shown](#)). This result suggests that the change in the AMO and PDO indices may contribute to the change
558 in the frequencies of the warm Arctic-cold Eurasia continent pattern.

559 3.7 Interdecadal variability

560 The four-decade-long ERA-Interim reanalysis is not adequate for examining interdecadal to
561 multi-decadal variations represented by the PDO and AMO indices. Further analysis is performed using
562 the 20CR daily reanalysis data for the 1854-2014 period. Before applying the SOM technique to the
563 20CR data, we first remove the trend to eliminate the influence from the global warming. No low-pass
564 filter is applied before SOM analysis in order to test the stability of the SOM results for the different
565 periods. The spatial SOM patterns from the de-trended century-long 20CR data (Figure 13) are similar
566 to those for the 1979-2019 period (Figure 1). Nodes 1, 4, and 7 correspond to the positive phase of the

567 warm Arctic-cold Eurasia pattern and the negative phase can be observed in nodes 3, 6, and 9. The
568 magnitude [in Figure 13](#) is smaller compared to the recent four decades [in Figure 1](#). The occurrence
569 frequencies of ~~all~~ the [four nodes, 1, 4, 6, and 9](#) (Figure 14), are close to those for the recent four
570 decades ([Figure 7](#)). It indicates that the SOM method can obtain stably the main modes of wintertime
571 surface air temperature variability. For the recent four decades, the time series of the number of days
572 also displays a noticeable increasing (decreasing) trend for nodes 1 and 4 (6 and 9), suggesting that the
573 trend in the recent four decades is a reflection of an interdecadal variability of wintertime surface air
574 temperature.

575 Next, we apply a 40-year low-pass filter to the time series of the occurrence frequencies for nodes
576 1, 4, 6 and 9 and the AMO and PDO indices and calculate correlations. There is a significant
577 correlation between the time series and the AMO index, with correlation coefficients of 0.36 for node 1,
578 0.27 for node 4, -0.37 for node 6, and -0.20 for node 9, all of which are at the 95% confidence level. No
579 significant correlations, however, are found between the filtered time series and the PDO index. If we
580 define ~~a~~ SST index to represent the variability of SST anomalies over the central North Pacific Ocean
581 (20°N-40°N, 150°E-150°W), the 40-year low-pass filtered central North Pacific Ocean SST index is
582 now significantly correlated with the filtered time series of occurrence frequencies for nodes 1 and 9
583 (0.55 for node 1 and -0.46 for node 9). The [correlation](#) results are consistent with the SST regression
584 map for the recent decades (Figure 10).

585 To confirm the effect of SST anomalies on the warm Arctic -cold Eurasia pattern, we also perform
586 EOF analysis of wintertime detrended seasonal surface air temperature anomalies for the 1854-2014
587 period (Figure 15). The spatial patterns of the first and second EOF modes show the negative phase of
588 the warm Arctic-cold Eurasia pattern and the 40-year low-pass filtered time series is inversely

589 correlated with the 40-year low-pass filtered wintertime AMO index (-0.46, $p < 0.05$ for mode 1 and
590 -0.44, $p < 0.05$ for mode 2). The 40-year low-pass filtered time series of the two EOF modes have a
591 significant negative correlation with the 40-year low-pass filtered central North Pacific Ocean SST
592 index, with correlation coefficients of -0.19 and -0.26 ($p < 0.05$). Only PC1 has a significant correlation
593 with the PDO index (0.38, $p < 0.05$). Thus, the increase in the occurrence of the warm Arctic-cold
594 Eurasia pattern in the recent decades is a part of the interdecadal variability of the pattern, which is
595 influenced by the AMO index, the PDO index, and the central North Pacific SST.

596 **4 Conclusions and Discussions**

597 In this study, we examine the variability of wintertime surface air temperature in the Arctic and the
598 Eurasian continent (20°E-130°E) by applying the SOM method to daily temperature from the gridded
599 ERA-Interim dataset for the period 1979-2019 and from the 20CR reanalysis for the period 1854-2014
600 and the EOF method to seasonal temperature from the 20CR reanalysis for the period 1854-2014. The
601 spatial pattern in the surface temperature variations in the study region, as revealed by the nine SOM
602 nodes, is dominated by concurrent warming in the Arctic and cooling in Eurasia, and vice versa. The
603 nine SOM patterns explain nearly 40% of the trends in wintertime surface temperature and 88% of that
604 are accounted for by only four nodes. Two of the four nodes (nodes 1 and 4) represent the warm
605 Arctic-cold Eurasian pattern and the other two (nodes 6 and 9) depict the opposite cold Arctic-warm
606 Eurasia pattern. There is a clear shift in the frequency of the occurrence of these patterns near the
607 beginning of this century, with the warm Arctic – cold Eurasia pattern dominating since 2003, while the
608 opposite pattern prevailing from the 1980s through the 1990s. The warm Arctic-cold Eurasia pattern is
609 accompanied by an anomalous high pressure and anticyclonic circulation over the Eurasian continent.
610 The anomalous winds and the associated temperature and moisture advection interact with local

611 | longwave radiative forcing and turbulent [fluxes](#) to produce positive (negative) temperature anomalies
612 | in the Arctic (Eurasian continent). The circulation is reversed for the cold Arctic-warm Eurasia pattern.
613 | The warm, moist air mass advected to the Arctic by the anomalous atmospheric circulations and the
614 | increased downward turbulent heat flux also explain sea ice melt in the Barents and Kara Seas. In other
615 | words, the sea ice loss in the Barents and Kara Seas and the cooling of the Eurasian continent can both
616 | be traced to anomalous atmospheric circulations.

617 | Increasing occurrences of the warm Arctic-cold Eurasian continent pattern appear to relate to
618 | rising SST over the central North Pacific and North Atlantic Oceans (positive AMO phase). The SST
619 | anomalies trigger two Rossby wavetrains spanning from the North Pacific Ocean, North America, and
620 | the North Atlantic Ocean to the Eurasian continent. The two wavetrains are strengthened through local
621 | sea-atmosphere-ice interactions in mid-high latitudes, which influence the change in the occurrence
622 | frequency of the warm Arctic-cold Eurasian continent pattern. Our results agree with those of previous
623 | studies (Lee et al., 2011; Sato et al., 2014; Clark and Lee, 2019). But previous studies only focus on the
624 | [effects](#) of SST anomalies over either North Pacific or North Atlantic Oceans. We also note that the two
625 | wavetrains excited by SST anomalies over different oceans differ in amplitudes, leading to somewhat
626 | different warm Arctic-cold Eurasia patterns.

627 | Using century-long data, we show that the warm Arctic-cold Eurasia pattern is an intrinsic climate
628 | mode, which has been stable since 1854. The recent increasing trend in its occurrence is a reflection of
629 | an interdecadal variability of the pattern resulting from the interdecadal variability of SST anomalies
630 | over the central Pacific Ocean and over the Atlantic Ocean represented by the AMO index. Sung et al.
631 | (2018) investigated interdecadal variability of the warm Arctic and cold Eurasia pattern and considered
632 | the variability of the SST over the North Atlantic as its origin. Our results suggest that the variability of

633 the SST over the North Pacific also plays an important role. However, internal atmospheric variability
634 remains another potential source. The Rossby wavetrains also lead to deepening of a trough in East
635 Asia and generate an anomalous low [pressure](#) and cold temperature in northern China ([Figure 10](#)),
636 which further suggests that ~~the relationship between~~ a warmer Arctic, especially warmer Barents and
637 Kara Seas ~~, and is not the driver for~~ the [increasing](#) occurrence of cold spells in East Asia, ~~as~~
638 ~~suggested in~~ ~~may not be as strong as~~ ~~previously thought studies~~ (Kim et al., 2014; Mori et al., 2014;
639 Kug et al., 2015; Overland et al., 2015).

640 ~~Our results suggest that the increasing trend in warm Arctic-cold Eurasia pattern may be related to~~
641 ~~the anomalous SST over the central North Pacific and the North Atlantic Oceans. But we cannot rule~~
642 ~~out the influence of the Arctic sea ice loss on the trend. Because the~~ ~~The Arctic sea ice loss results from~~
643 ~~two main drivers: external and internal forcings. The former refers to the both Arctic warming due to~~
644 ~~anthropogenic increasing of greenhouse gas concentrations and natural variability of ; the latter comes~~
645 ~~from the climate system internal variability, such as anomalous SST anomalies. This study considers~~
646 ~~natural variability or only the internal driver of climate system. The Arctic warming caused external~~
647 ~~forcing related to increasing greenhouse gas emissions can produce an anomalous anticyclone over the~~
648 ~~Barents and Kara Seas, leading to the warm Arctic-cold continents pattern.~~

649 ~~Although the ERA-Interim reanalysis is overall superior in describing~~ ~~has the best performance in~~
650 ~~overall depiction of the Arctic atmospheric environment to other similar global reanalysis products, it~~
651 ~~contains~~ ~~includes~~ ~~warm and moist biases in the surface layer~~ (Jakobson et al., 2012; Chaudhuri et al.,
652 ~~2014; Simmons and Poli, 2015; Wang et al., 2019). However, we believe these biases, as well as the~~
653 ~~relatively coarse resolution, should have minimum impact in the results from the current analyses.~~
654 ~~Further, although the current analyses were performed on a predetermined SOM grid with 3x3 nodes,~~

655 [an increase in the number of SOM nodes didn't change the conclusions.](#)

656 Our results help broaden the current understanding of the formation mechanisms for the warm
657 Arctic-cold Eurasia pattern. The SST anomalies over Northern Hemisphere oceans may offer a
658 potential for predicting its occurrence. [The statistical relationship between SST anomalies and the
659 occurrences of the warm Arctic-cold continents pattern may help improve the predictability of
660 wintertime surface air temperature over Eurasian continent on interdecadal time scales.](#)

661 **Data Availability**

662 All data used in the current analyses are publicly available. The monthly sea ice concentration data are
663 available from the National Snow and Ice Data Center (NSIDC) (<http://nsidc.org/data/NSIDC-0051>), the
664 ERA-Interim reanalysis data are available from the European Center for Mid-Range Weather
665 Forecasting (<https://www.ecmwf.int/en/forecasts/datasets/reanalysis-datasets/era-interim>) and the sea
666 surface temperature data are available from the Hadley Centre for Climate Prediction and Research
667 (<ftp://ftp.cdc.noaa.gov/Datasets/noaa.oisst.v2.highres/>). The long-term SST data are derived from
668 from the Twentieth Century Reanalysis project, version 2c (20CR)
669 (<https://climatedataguide.ucar.edu/climate-data/noaa-20th-century-reanalysis-version-2-and-2c>).

670 **Competing interests**

671 The authors declare that they have no conflict of interest.

672 **Author Contributions**

673 L. Yu designed the study, with input from S. Zhong, and carried out the analyses. L. Yu and S. Zhong
674 prepared the manuscript. C. Sui plotted a part of Figures. [-B. Sun revised the manuscript.](#)

675 **Acknowledgements** We thank the European Centre for Medium-Range Weather Forecasts (ECMWF)
676 for the ERA-Interim data. This study is financially supported by the National Key R&D Program of
677 China (2019YFC1509102; 2017YFE0111700) and the National Natural Science Foundation of China
678 (41922044).

679

680

681

682

683

684

685

686

687

688

689

690 **References**

691 Barnes, E. A. and Screen, J. A.: The impact of Arctic warming on the midlatitude jet-stream: Can it?

692 Has it? Will it?, WIREs Clim. Change, 6, 277-286, doi:10.1002/wcc.337, 2015.

693 Blackport, R., Screen J. A., Wiel K. van der, and Bintanja, R.: Minimal influence of reduced Arctic sea

694 ice on coincident cold winters in mid-latitudes, Nature Climate Change, 9,

695 doi:10.1038/s41558-019-0551-4, 2019, 2019.

696 [Chaudhuri, A. H., Ponte, R. M., and Nguyen, A. T.: A Comparison of atmospheric reanalysis products](#)

697 [for the Arctic Ocean and implications for uncertainties in air-sea fluxes, J. Climate, 27,](#)

698 [5411-5421, doi:10.1175/JCLI-D-13-00424.1, 2014.](#)

699 [Chen, L., Francis J. and Hanna E.: The “Warm-Arctic/Cold continents” pattern during 1901-2010.](#)

700 [Int. J. Climatol., 38, 5245-5254, ~~https://doi.org/doi:10.1002/joc.5725~~, 2018.](#)

701 Clark, J. P. and Lee, S.: The role of the tropically excited Arctic Warming Mechanism on the warm

702 Arctic cold continent surface air temperature trend pattern, *Geophys. Res. Lett.*, 46, 8490-8499,
703 doi:10.1029/2019GL082714, 2019

704 Cohen, J., Screen, J. A., Furtado, J. C., Barlow, M., Whittleston, D., Coumou, D., Francis, J., Dethloff,
705 K., Entekhabi, D., Overland, J., and Jones, J.: Recent Arctic amplification and extreme
706 mid-latitude weather, *Nat. Geosci.*, 7, 627-637, doi:10.1038/ngeo2234, 2014.

707 Cohen, J., Pfeiffer, K., and Francis, J. A.: Warm Arctic episodes linked with increased frequency of
708 extreme winter weather in the United States, *Nat. Commun.*, 9, 869,
709 doi:10.1038/s41467-018-02992-9, 2018.

710 Compo, G. P., Whitaker, J. S., Sardeshmukh, P. D., Matsui, N., Allan, R., Yin, X., Jr, G. B. E., Vose, R.
711 S., Rutledge, G. K., Bessemoulin, P., Brönnimann, S., Brunet, M., Crouthamel, R. I., Grant, A.
712 N., Groisman, P. Y., Jones, P. D., Kruk, M. C., Kruger, A. C., Marshall, G. J., Maugeri, M., Mok,
713 H. Y., Nordli, Ø., Ross, T. F., Trigo, R. M., Wang, X., Woodruff, S. D., and Worley S. J.: The
714 Twentieth Century Reanalysis Project, *Quart. J. Roy. Meteor. Soc.*, 137, 1-28,
715 doi:10.1002/qj.776, 2011.

716 Dee, D. P., Uppala, S. M., Simmons, A. J., Berrisford, P., Poli, P., Kobayashi, S., Andrac, U.,
717 Balsameda, M. A., Balsamo, G., Bauer, P., Bechtold, P., Beljaars, A. C. M., van de Berg, L.,
718 Bidlot, J., Bormann, N., Delsol, C., Dragani, R., Fuentes, M., Geer, A. J., Haimberger, L., Healy,
719 S. B., Hersbach, H., Hõm, E. V., Isaksen, L., Kålberg, P., Köhler, Matricardi, M., McNally, A.
720 P., Monge-Sanz, B. M., Morcrette, J.-J., Park, B.-K., Peubey, C., de Rosnay, P., Tavolato, C.,
721 Thépaut, J.-N., and Vitart, F.: The ERA-Interim reanalysis: configuration and performance of the
722 data assimilation system. *Q. J. R. Meteorol. Soc.*, 137, 553-597, doi:10.1002/qj.828, 2011.

723 Enfield, D. B., Mestas-Nunez, A. M., and Trimble, P. J.: The Atlantic multidecadal oscillation and it's

724 relation to rainfall and river flows in the continental U.S., *Geophys. Res. Lett.*, 28, 2077-2080,
725 2001.

726 Fyfe, J. C.: Midlatitudes unaffected by sea ice loss. *Nature Climate Change*, 9,
727 doi:10.1038/s41558-019-0560-3, 2019 .

728 Gibson, P. B., Perkins-Kirkpatrick, S. E., Uotila, P., Pepler, A. S., and Alexander, L. V.: On the use of
729 self-organizing maps for studying climate extremes, *J. Geophys. Res. Atmos.*, 122, 3891–3903,
730 [doi:10.1002/2016JD026256](https://doi.org/10.1002/2016JD026256), 2017.

731 Hoskins, B. and Woollings, T.: Persistent extratropical regimes and climate extremes. *Curr. Clim. Change*
732 *Rep.*, 1, 115-124, doi:10.1007/s40641-015-0020-8, 2015

733 Horton, D. E., Johnson, N. C., Singh, D., Swain, D. L., Rajaratnam, B., and Diffenbaugh, N. S.:
734 Contribution of changes in atmospheric circulation patterns to extreme trends, *Nature*,
735 522,465-469, doi:10.1038/nature14550, 2015.

736 Inoue, J., Hori, M. E., and Takaya, K.: The role of Barents Sea ice in the wintertime cyclone track and
737 emergence of a warm-Arctic-Siberian anomaly, *J. Clim.*, 25, 2561-2568,
738 doi:10.1175/JCLI-D-11-00449.1, 2012.

739 Jakobson, E., Vihma, T., Palo, T., Jakobson, L., Keernik, H., and Jaagus, J.: Validation of atmospheric
740 reanalyses over the central Arctic Ocean, *Geophys. Res. Lett.*, 39, L10802,
741 doi:10.1029/2012GL051591, 2012.

742 Johnson, N. C. and Feldstein, S. B.: The continuum of North Pacific sea level pressure patterns:
743 Intraseasonal, interannual, and interdecadal variability, *J. Clim.*, 23,
744 851-867, doi:10.1175/2009JCLI3099.1, 2010.

745 [Jakobson, E., Vihma, T., Palo, T., Jakobson, L., Keernik, H., Jaagus, J.: Validation of atmospheric](#)

746 | [reanalyses over the central Arctic Ocean, Geophys. Res. Lett., 39, 2012.](#)

747 Kalnay, E., Kanamitsu, M., Kistler, R., Collins, W. G., Deaven, D., Gandin, L., Iredell, M., Saha, S.,
748 White, G., Woollen J.: The NCEP/NCAR 40-year reanalysis project, Bull. Amer. Meteor. Soc.,
749 77, 437-471, doi:10.1175/1520-0477(1996)077<0437:TNYRP>2.0.CO;2, 1996.

750 Kim, B.-M., Son, S.-W., Min, S.-K., Jeong, J.-H., Kim, S.-J., Zhang, X., Shim, T., and Yoon, J.-H.:
751 Weakening of the stratospheric polar vortex by Arctic sea-ice loss, Nature Commun., 5, 4646,
752 doi:10.1038/ncomms5646, 2014.

753 Kohonen, T.: Self-Organizing Maps. 3rd ed. Springer, 501 pp, 2001.

754 Kug, J.-S., Jeong, J.-H., Jang, Y.-S., Kim, B.-M., Folland, C. K., Min, S.-K., and Son, S.-W.: Two
755 distinct influences of Arctic warming on cold winters over North America and East Asia, Nat.
756 Geosci., 8, 759-762, doi:10.1038/ngeo2517, 2015.

757 Lee, S., Gong, T., Johnson, N., Feldstein, S. B., and Pollard, D.: On the possible link between tropical
758 convection and the Northern Hemisphere Arctic surface air temperature change between 1958
759 and 2001, J. Clim., 24, 4350-4367, doi:10.1175/2011JCLI4003.1, 2011.

760 Lee, S. and Feldstein, S. B.: Detecting ozone- and greenhouse gas-driven wind trends with
761 | observational data, Science, 339, 563-567, [doi:10.1126/science.1225154](#), 2013.

762 Loikith, P. C. and Broccoli, A. J.: Comparison between observed and model-simulated atmospheric
763 circulation patterns associated with extreme temperature days over North America using CMIP5
764 historical simulations, J. Clim., 28, 2063-2079, doi:10.1175/JCLI-D-13-00544.1, 2015.

765 Luo, D., Xiao, Y., Yao, Y., Dai, A., Simmonds, I., and Franzke, C. L. E.: Impact of Ural blocking on
766 winter warm Arctic-cold Eurasian anomalies. Part I: Blocking-induced amplification, J. Clim.,
767 29, 3925-3947, doi:10.1175/JCLI-D-15-0611.1, 2016.

768 Mantua, N. J., Hare, S. R., Zhang, Y., Wallace, J. M., and Francis, R. C.: A Pacific interdecadal climate
769 oscillation with impacts on salmon production, *Bull. Amer. Meteor. Soc.*, 78, 1069–1079, 1997.

770 Matsumura, S. and Kosaka, Y.: Arctic-Eurasian climate linkage induced by tropical ocean variability,
771 *Nature Communications*, 10, 3441, doi:10.1038/s41467-019-11359-7, 2019.

772 Mori, M., Watanabe, M., Shiogama, H., Inoue, J., and Kimoto, M.: Robust Arctic sea-ice influence on
773 the frequent Eurasian cold winters in past decades, *Nat. Geosci.*, 7, 869-873,
774 doi:10.1038/ngeo2277, 2014.

775 Mori, M., Kosaka, Y., Watanabe, M., Nakamura, H., and Kimoto, M.: A reconciled estimate of the
776 influence of Arctic sea-ice loss on recent Eurasian cooling, *Nat. Clim. Change*, 9, 123-129,
777 doi:10.1038/s41558-018-0379-3, 2019.

778 McCusker, K. E., Fyfe, J. C., and Sigmond, M.: Twenty-five winters of unexcepted Eurasian cooling
779 unlikely due to Arctic sea-ice loss, *Nat. Geosci.*, 9, 838-842, doi:10.1038/ngeo2820, 2016.

780 Overland, J. E., Wood, K. R., and Wang, M.: Warm Arctic-cold continents: climate impacts of the
781 newly open Arctic sea, *Polar Res.*, 30, 15787, doi:10.3402/polar.v30i0.15787, 2011.

782 Overland, J. E., Francis, J., Hall, R., Hanna, E., Kim, S.-J., and Vihma, T.: The melting Arctic and
783 Midlatitude weather patterns: Are they connected?, *J. Clim.*, 28, 7917-7932,
784 doi:10.1175/JCLI-D-14-00822.1, 2015.

785 Palmer, T. N.: A nonlinear dynamical perspective on climate prediction, *J. Clim.*, 12, 575-591, 1999.
786 doi:10.1175/1520-0442(1999)012<0575:ANDPOC>2.0.CO;2

787 Peings, Y.: Ural blocking as a driver of early-winter stratospheric warmings, *Geophys. Res. Lett.*, 46,
788 5460-5468, doi:10.1029/2019GL082097, 2019.

789 Reusch, D. B., Alley, R. B., and Hewitson, B. C.: Relative performance of self-organizing maps and

790 principal component analysis in pattern extraction from synthetic climatological data, *Polar*
791 *Geogr.*, 29, 188–212, doi:10.1080/789610199, 2005.

792 Reynolds, R. W., Smith, T. M., Liu, C., Chelton, D. B., Casey, K. S., Schlax, M. G.: Daily
793 High-Resolution-Blended Analyses for Sea Surface Temperature, *J. Climate*, 20, 5473-5496,
794 doi:10.1175/2007JCLI1824.1, 2007.

795 Sammon, J. W.: A non-linear mapping for data structure analysis. *IEEE Trans. Computers*, C-18,
796 401–409 , 1969.

797 Sato, K., Inoue, J., and Watanabe, M.: Influence of the Gulf Stream on the Barents Sea ice retreat and
798 Eurasian coldness during early winter, *Environ. Res. Lett.*, 9, 084009,
799 doi:10.1088/1748-9326/9/8/084009, 2014.

800 Schudeboom, A., McDonald, A. J., Morgenstern, O., Harvey, M., and Parsons, S.: Regional
801 regime-based evaluation of present-day GCM cloud simulations using self-organizing maps, *J.*
802 *Geophys. Res. Atmos.*, 123, 4259–4272, doi:10.1002/2017JD028196, 2018.

803 Screen, J. A. and Simmonds, I.: The central role of diminishing sea ice in recent Arctic temperature
804 amplification, *Nature*, 464, 1334-1337, doi:10.1038/nature09051, 2010.

805 Screen, J. S. and Simmonds, I.: Erroneous Arctic temperature trends in the ERA-40 reanalysis: A closer
806 look, *J. Clim.*, 24, 2620–2627, doi:10.1175/2010JCLI4054.1, 2011.

807 Sedlar, J., Tjernström, M., Mauritsen, T., Shupe, M. D., Brooks, I. M., Persson, O., Birch, C. E., Leck,
808 C., Sirevaag, A., and Nicolaus, M. : A transitioning Arctic surface energy budget: The impacts of
809 solar zenith angle, surface albedo and cloud radiative forcing, *Clim. Dyn.*, 37, 1643–1660,
810 [doi:10.1007/s00382-010-0937-5](https://doi.org/10.1007/s00382-010-0937-5), 2011.

811 Shepherd, T. G.: Effects of a warming Arctic, *Science*, 353, 989-990, doi:10.1126/science.aag2349,

812 2016.

813 [Simmons, A., and Poli, P.: Arctic warming in ERA-Interim and other analyses, Q. J. R. Meteorol. Soc.,](#)
814 [141, 1147-1162, doi:10.1002/qj.2422, 2015.](#)

815 Skific, N., Francis, J. A., and Cassano, J. J.: Attribution of projected changes in atmospheric moisture
816 transport in the Arctic: A self-organizing map perspective, *J. Clim.*, 22, 4135-4153,
817 doi:10.1175/2009JCLI2645.1, 2009.

818 Sorokina, S. A., Li, C., Wettstein, J. J., and Kvamstø, N. G.: Observed atmospheric coupling between
819 Barents sea ice and the warm-Arctic cold-Siberian anomaly pattern, *J. Clim.*, 29, 495-511,
820 doi:10.1175/JCLI-D-15-0046.1, 2016.

821 Stroeve, J. C., Holland, M. M., Meier, W., Scambos, T., and Serreze, M.: Arctic sea ice decline: faster
822 than forecast, *Geophys. Res. Lett.*, 34, L09051, doi:10.1029/2007gl029703, 2007.

823 Stroeve, J. C.: Trends in Arctic sea ice extent from CMIP5, CMIP3 and observations, *Geophys. Res.*
824 *lett.*, 39, L16502, doi:10.1029/2012GL052676, 2012.

825 Sun, L., Perlwitz, J., and Hoerling, M.: What caused the recent “warm Arctic-Cold Continents” trend
826 pattern in winter temperature?, *Geophys. Res. Lett.*, 43, 5345-5352,
827 doi:10.1002/2016GL069024, 2016.

828 Sung, M.-K., Kim, S.-H., Kim, B.-M., and Choi, Y.-S.: Interdecadal variability of the warm Arctic and
829 cold Eurasia pattern and its North Atlantic origin, *Journal of Climate*, 31, 5793-5810,
830 doi:10.1175/JCLI-D-17-0562.1, 2018.

831 Tang, Q., Zhang, X., Yang, X., and Francis J. A.: Cold winter extremes in northern conditions linked to
832 Arctic sea ice loss, *Environ. Res. Lett.*, 8, 014036, doi:10.1088/1748-9326/8/1/014036, 2013.

833 Takaya K, and Nakamura, H.: A formulation of a phase-independent wave-activity flux for stationary

834 and migratory quasigeostrophic eddies on a zonally varying basic flow, *J. Atmos. Sci.*, 58,
835 608-627, 2001.

836 Uppala, S., KÅllberg, P. W., Simmons, A. J., Andrae, U., Da Costa Bechtold, V., Florino, M., Gibson, J.
837 K., Haseler, J., Hernandez, A., Kelly, G. A., Li, X., Onogi, K., Saarinen, S., Sokka, N., Allan, R.
838 P., Andersson, E., Arpe, K., Balmaseda, M. A., Beljaars, A. C. M., Van De Berg, L., Bidlot, J.,
839 Bormann, N., Caires, S., Chevallier, F., Dethof, A., Dragosavac, M., Fisher, M., Fuentes, M.,
840 Hagemann, S., Hm, E., Hoskins, B. J., Isaksen, L., Janssen, P. A. E. M., Jenne, R., McNally, A.
841 P., Mahfouf, J.-F., Morcrette, J.-J., Rayner, N. A., Saunders, R. W., Simon, P., Sterl, A.,
842 Trenberth, K. E., Untch, A., Vasiljevic, D., Viterbo, P., and Woollen, J.: The ERA-40 re-analysis,
843 *Quarterly Journal of the Royal Meteorological Society*, 131, 2961–3012, doi:10.1256/qj.04.176,
844 2005.

845 Walsh, J. E.: Intensified warming of the Arctic: Causes and impacts on middle Latitudes, *Glob. Planet.*
846 *Change*, 117, 52-63, doi:10.1016/j.gloplacha.2014.03.003 , 2014.

847 Vihma, T.: Effects of Arctic sea ice decline on weather and climate: A review, *Surv. Geophys.*, 35,
848 1175-1214, doi:10.1007/s10712-014-9284-0 , 2014.

849 Vihma, T., Graverson, R., Chen, L., Handorf, D., Skific, N., Francis, J. A., Tyrrell, N., Hall, R., Hanna,
850 E., Uotila, P., Dethloff, K., Karpechko, A. Y., Björnsson, H., and Overland, J. E.: Effects of the
851 tropospheric large-scale circulation on European winter temperatures during the period of amplified
852 Arctic warming, *Int. J. Climatol.*, doi:10.1002/joc.6225, 2019.

853 [Wang, C., Graham, R. M., Wang, K., Gerland, S., Granskog, M. A.: Comparison of ERA5 and](#)
854 [ERA-Interim near-surface air temperature, snowfall and precipitation over Arctic sea ice: effects](#)
855 [on sea ice thermodynamics and evolution, *The Cryosphere*, 13, 1661-1679, 2019.](#)

856 Yoo, C., Feldstein, S., and Lee, S.: The impact of the Madden–Julian oscillation trend on the Arctic
857 amplification of surface air temperature during the 1979–2008 boreal winter, *Geophys. Res.*
858 *Lett.*, 38, L24804, doi:10.1029/2011GL049881, 2011.

859 Yu, L., Zhong, S., Winkler, J. A., Zhou, M., Lenschow, D. H., Li, B., Wang, X., and Yang, Q.: Possible
860 connections of the opposite trends in Arctic and Antarctic sea-ice cover, *Scientific Reports*, 7,
861 45804, doi:10.1038/srep45804, 2017.

862

863

864

865 Table 1. Spatial correlations (Corrs) between the daily winter (DJF) surface air
 866 temperature and the corresponding SOM pattern for each day from 1979 to 2018.

	3×1	2×2	3×2	4×2	3×3	5×2	4×3	5×3	4×4
Corr	0.26	0.43	0.48	0.48	0.50	0.49	0.50	0.51	0.51

867

868

869

870

871

872

873

874

875

876

877

878

879

880

881

882

883

884

885

886

887

888

889

890

891

892

893

894

895

896

897 Table 2. Averaged anomalous NAO and AO indices for all occurrences of each SOM
 898 node. Asterisks indicate the above 95% confidence level.
 899

	Node1	Node2	Node3	Node4	Node5	Node6	Node7	Node8	Node9
NAO	0.38*	0.22*	0.12*	0.05	-0.22*	-0.02	-0.07	-0.31*	-0.32*
AO	0.44*	0.38*	1.03*	-0.42	-0.62*	0.22*	-0.44*	-1.11*	-0.41*

900
 901
 902
 903
 904
 905
 906
 907
 908
 909
 910
 911
 912
 913
 914
 915
 916
 917
 918
 919
 920
 921
 922
 923
 924
 925
 926
 927
 928
 929
 930
 931
 932
 933
 934
 935
 936
 937

938 Table 3. Trends in the frequency of occurrences for each SOM node (day yr⁻¹).
939 Asterisks indicate the above 95% confidence level.

940

	Node1	Node2	Node3	Node4	Node5	Node6	Node7	Node8	Node9
Trend	0.80*	0.10	-0.18	0.22*	-0.02	-0.39*	0.17	-0.17	-0.50*

941

942

943

944

945

946

947

948

949

950

951

952

953

954

955

956

957

958

959

960

961

962

963

964

965

966

967

968

969

970

971

972

973

974

975

976

977

978 Table 4. Frequencies of occurrence (%) of wintertime surface air temperature patterns
 979 in Figure 1 for all winters before 1998 and after 1998 for the period 1979-2019.
 980 Values with Asterisks are significantly different from climatology above the 95%
 981 confidence level.
 982

SOM patterns	Frequencies of occurrence		
	All winters	Winters before 1998	Winters after 1998
Node 1	17.1	7.4*	26.8
Node 2	4.4	3.3	5.4
Node 3	17.2	18.8	15.6
Node 4	8.6	5.4	11.7
Node 5	3.4	3.4	3.5
Node 6	10.2	15.2*	2.1*
Node 7	13.7	10.6	16.8
Node 8	10.1	12.1	8.0
Node 9	15.4	23.7*	7.1*

983
 984
 985
 986
 987
 988
 989
 990
 991
 992
 993
 994
 995
 996
 997
 998
 999
 1000
 1001
 1002
 1003
 1004
 1005
 1006
 1007
 1008
 1009

1010 **Figure Captions**

1011 Figure 1. Spatial patterns of SOM nodes for daily wintertime (December, January, and
1012 February) surface air temperature anomalies (°C) without removing their linear trends
1013 from ERA-Interim reanalysis over the 1979-2019 period. The number in brackets
1014 denotes the frequency of the occurrence for each node.

1015 Figure 2. Corresponding 500-hPa geopotential height anomalies (gpm) without
1016 removing their linear trends from ERA-Interim reanalysis over the 1979-2019 period
1017 for each node in Figure 1. Dotted regions indicate the above 95% confidence level.
1018 The thick black lines show the study region.

1019 Figure 3. Corresponding anomalous 850-hPa wind field (ms^{-1}) without removing ~~the~~
1020 its linear trend from ERA-Interim reanalysis over the 1979-2019 period for each node
1021 in Figure 1. Shaded regions indicate the above 95% confidence level. The thick black
1022 lines show the study region.

1023 Figure 4. Corresponding anomalous daily accumulated downward longwave radiation
1024 (105 W m^{-2}) without removing ~~the~~ its linear trend from ERA-Interim reanalysis over
1025 the 1979-2019 period for each node in Figure 1. Dotted regions indicate the above 95%
1026 confidence level. The thick black lines denote show the study region.

1027 Figure 5. Corresponding anomalous daily accumulated turbulent heat flux (sensible
1028 and latent heat) (10^5 W m^{-2}) without removing their linear trends from ERA-Interim
1029 reanalysis over the 1979-2019 period for each node in Figure 1. Positive values
1030 denote heat flux from atmosphere to ocean and vice versa. Dotted regions indicate the
1031 above 95% confidence level. The thick black lines denote show the study region.

1032 Figure 6. Corresponding anomalous wintertime sea ice concentration without
1033 removing ~~the-its linear~~ trend from the NSIDC over the 1979-2019 period for each
1034 node in Figure 1. Dotted regions indicate the above 95% confidence level.

1035 Figure 7. Time series of the number of days for occurrence of each SOM node in
1036 Figure 1 over the 1979-2019 period. The thick lines denote the trend in time series.

1037 Figure 8. Total (top), SOM-explained (middle), and residual (bottom) trend in
1038 wintertime (DJF) surface air temperature ($^{\circ}\text{C yr}^{-1}$) over the 1979-2019 period. Dots in
1039 the top panel indicate above 95% confidence level.

1040 Figure 9. Trends in surface air temperature explained by each SOM node ($^{\circ}\text{C yr}^{-1}$)
1041 over the 1979-2019 period. The percentage in the upper of each panel indicates the
1042 fraction of the total trend represented by each node.

1043 Figure 10. Anomalous SST ($^{\circ}\text{C}$) regressed into the normalized time series of
1044 occurrence number for nodes 1, 4, 6, and 9 without removing ~~the-its linear~~ trend from
1045 the NOAA over the 1979-2019 period.

1046 Figure 11. Anomalous 500-hPa geopotential height (gpm) regressed into the
1047 normalized time series of occurrence number for nodes 1, 4, 6, and 9 without
1048 removing ~~the-its linear~~ trend from ERA-Interim reanalysis over the 1979-2019 period.

1049 Figure 12. The anomalous wave activity flux (vectors) (Takaya and Nakamura, 2001)
1050 and stream function (colors, units: $10^7 \text{ m}^2 \text{ s}^{-1}$) regressed onto the normalized time
1051 series of occurrence number for nodes 1, 4, 6, and 9 without removing ~~the-their linear~~
1052 trends from ERA-Interim reanalysis over the 1979-2019 period.

1053 Figure 13. Spatial patterns of SOM nodes for detrended daily wintertime (December,

1054 January, and February) surface air temperature anomalies ($^{\circ}\text{C}$) from the 20CR
1055 reanalysis for the 1851-2014 period. The number in brackets denotes the frequency of
1056 the occurrence for each node.

1057 Figure 14. Time series of the number of days for occurrence of each SOM node in
1058 Figure 13 from the 20CR reanalysis for the 1851-2014 period. The thick red lines
1059 denote the result in Figure 7 from the ERA-Interim reanalysis for the 1979-2019
1060 period.

1061 Figure 15. The (a) leading pattern and (b) its time series (PC1 and PC2) of EOF
1062 analysis of wintertime surface air temperature anomalies from the 20CR reanalysis for
1063 the 1851-2014 period. Prior to EOF analysis, surface air temperature data are
1064 detrended. A 40-yr low-pass filter is applied to the time series of PC1, PC2, AMO,
1065 PDO, and central North Pacific Ocean (CNPO) indices. The correlation coefficients
1066 between PC1 and AMO, PDO and CNPO indices are -0.46 ($p < 0.0001$), 0.38
1067 ($p < 0.0001$), and -0.19 ($p = 0.019$); those between PC2 and AMO, PDO and CNPO
1068 indices are -0.44 ($p < 0.0001$), 0.38 ($p < 0.0001$), and -0.26 ($p = 0.0009$).

1069

1070

1071

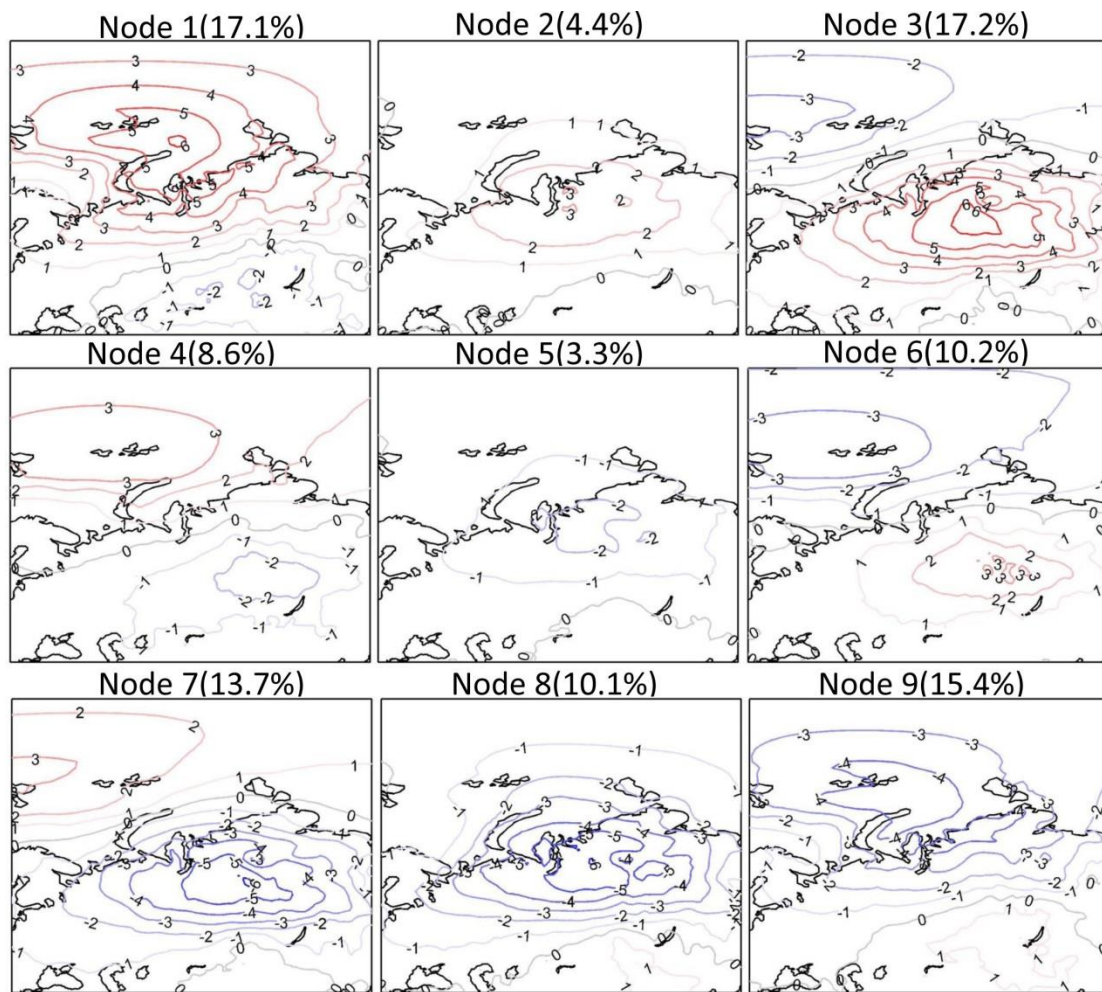
1072

1073

1074

1075

1076



1077

1078 Figure 1. Spatial patterns of SOM nodes for daily wintertime (December, January, and February)
1079 surface air temperature anomalies (°C) without removing their linear trends from ERA-Interim
1080 reanalysis over the 1979-2019 period. The number in brackets denotes the frequency of the
1081 occurrence for each node.

1082

1083

1084

1085

1086

1087

1088

1089

1090

1091

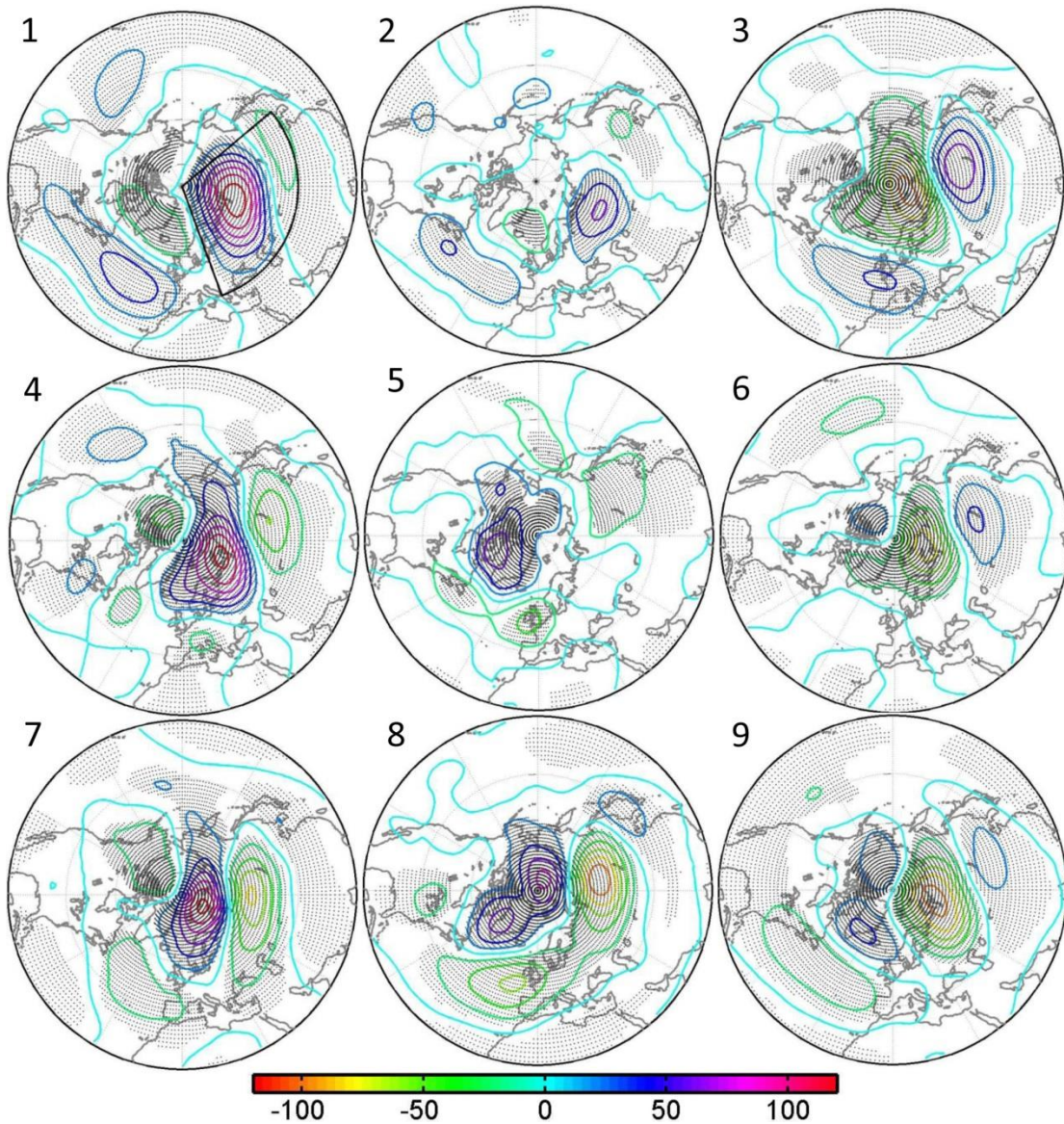
1092

1093

1094

1095

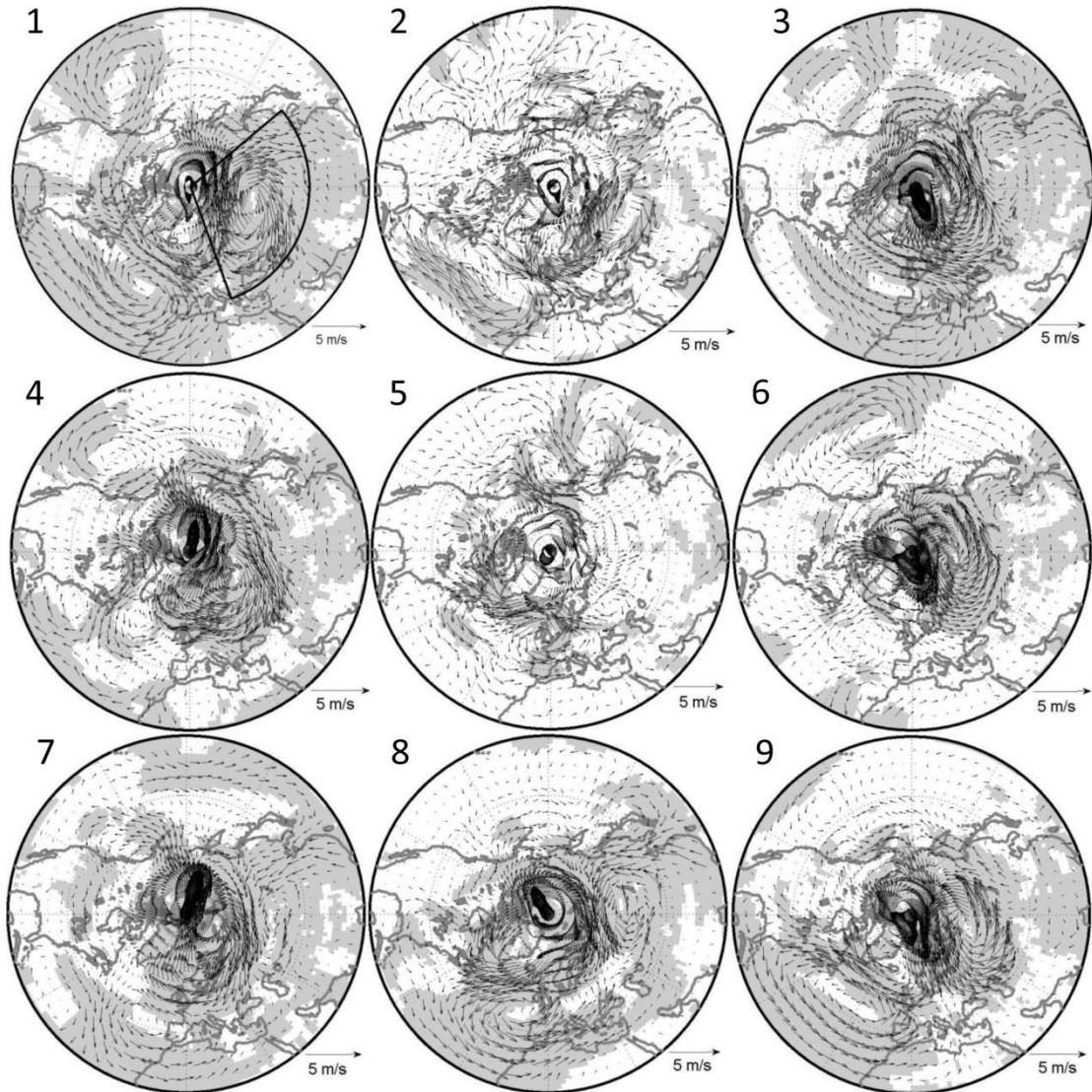
1096



1098
 1099
 1100
 1101
 1102
 1103
 1104
 1105
 1106
 1107
 1108
 1109
 1110
 1111
 1112
 1113

Figure 2. Corresponding 500-hPa geopotential height anomalies (gpm) without removing their linear trends from ERA-Interim reanalysis over the 1979-2019 period for each node in Figure 1. Dotted regions indicate the above 95% confidence level. The thick black lines denote-show the study region.

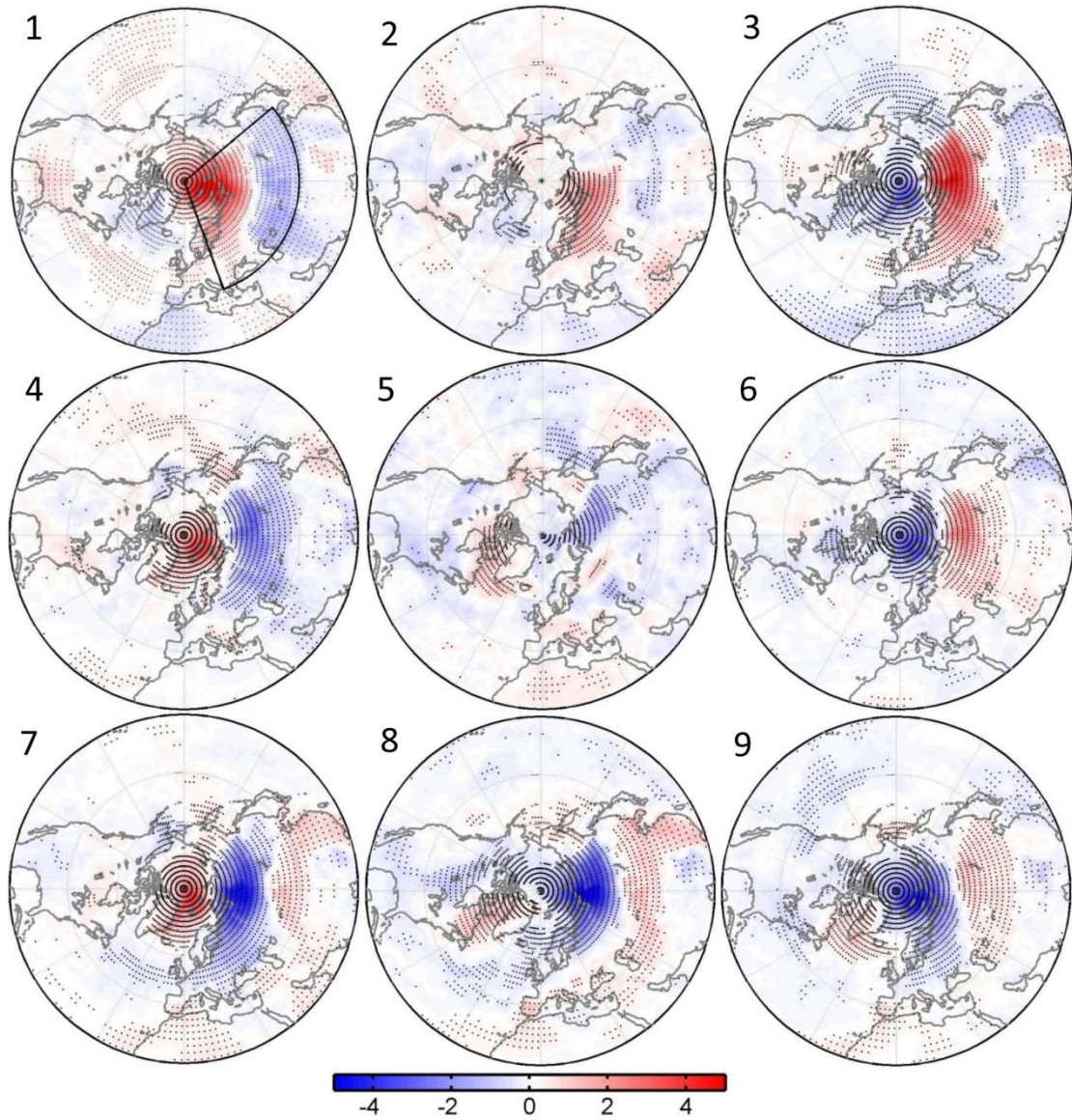
1114
1115
1116



1117
1118
1119
1120
1121
1122
1123
1124
1125
1126
1127
1128
1129
1130
1131

Figure 3. Corresponding anomalous 850-hPa wind field ~~(ms^{-1})~~ without removing its linear trend from ERA-Interim reanalysis over the 1979-2019 period for each node in Figure 1. Shaded regions indicate the above 95% confidence level. The thick black lines ~~denotes~~ show the study region.

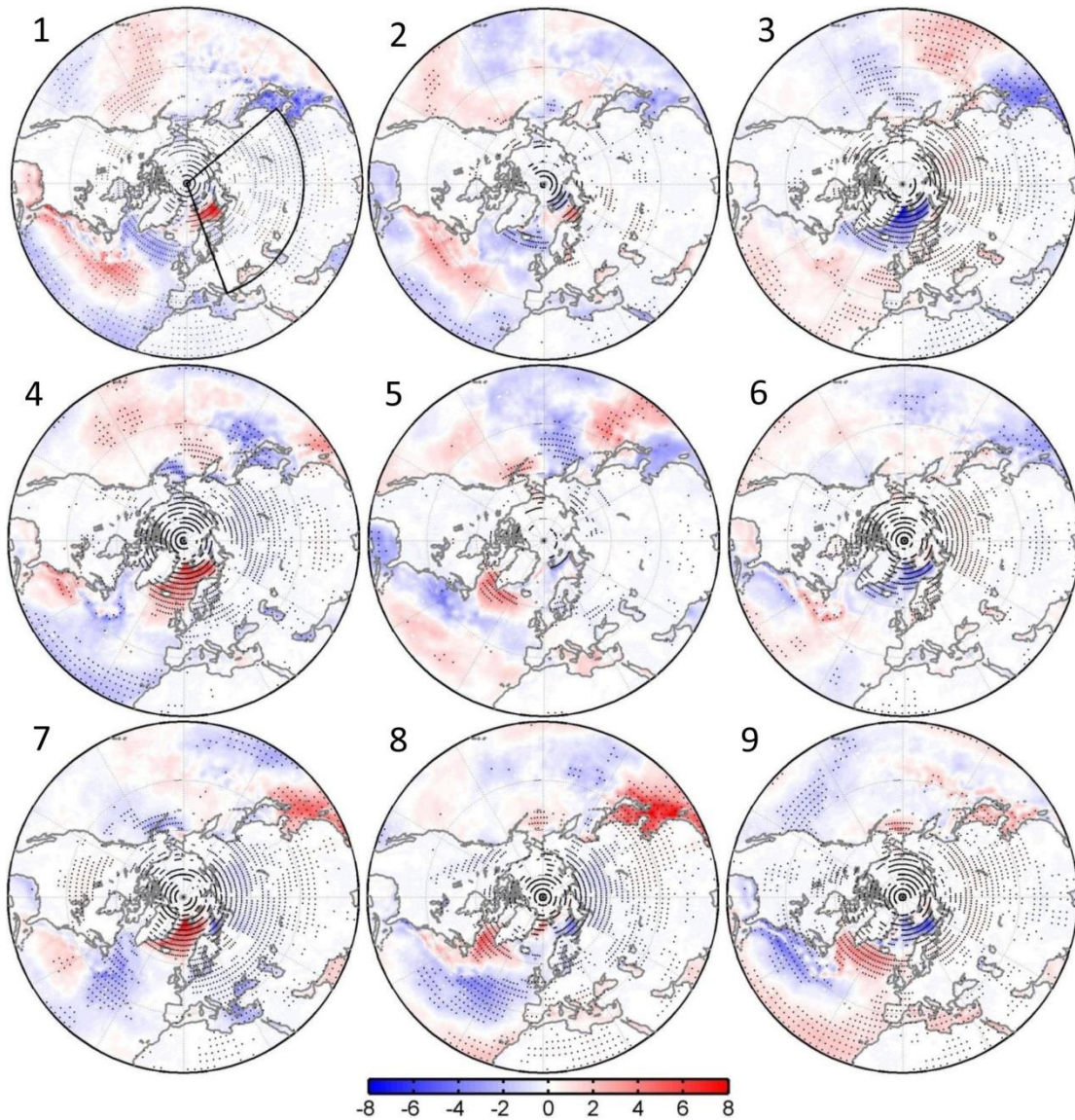
1132
1133
1134
1135
1136
1137



1138
1139
1140
1141
1142
1143
1144
1145
1146
1147
1148

Figure 4. Corresponding anomalous daily accumulated downward longwave radiation (10^5 W m^{-2}) without removing its linear trend from ERA-Interim reanalysis over the 1979-2019 period for each node in Figure 1. Dotted regions indicate the above 95% confidence level. The thick black lines denote show the study region.

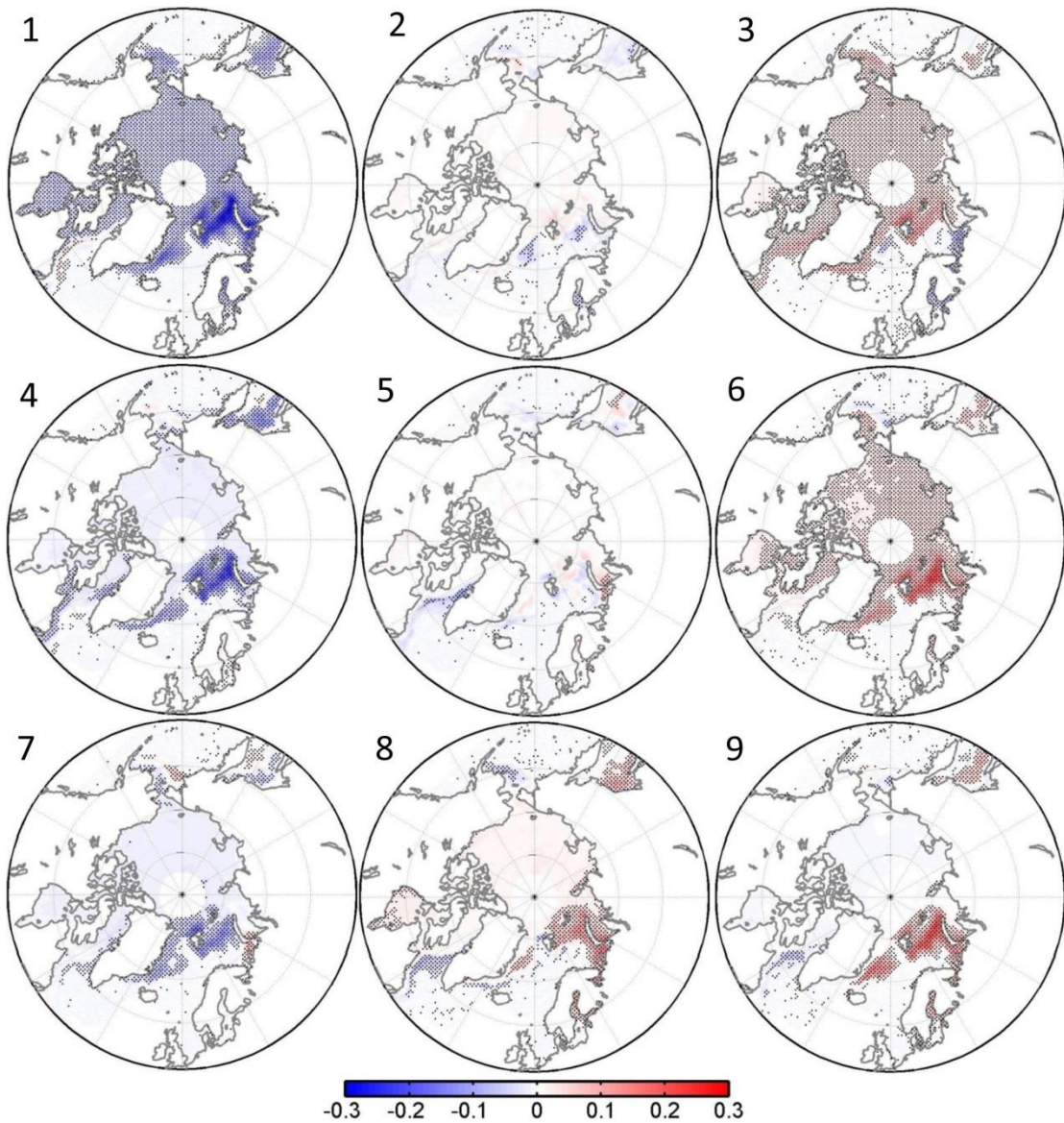
1149
1150
1151
1152
1153
1154
1155
1156
1157



1158
1159
1160
1161
1162
1163
1164
1165

Figure 5. Corresponding anomalous daily accumulated turbulent heat flux (sensible and latent heat) (10^5 W m^{-2}) without removing their linear trends from ERA-Interim reanalysis over the 1979-2019 period for each node in Figure 1. Positive values denote heat flux from atmosphere to ocean and vice versa. Dotted regions indicate the above 95% confidence level. The thick black lines denote show the study region.

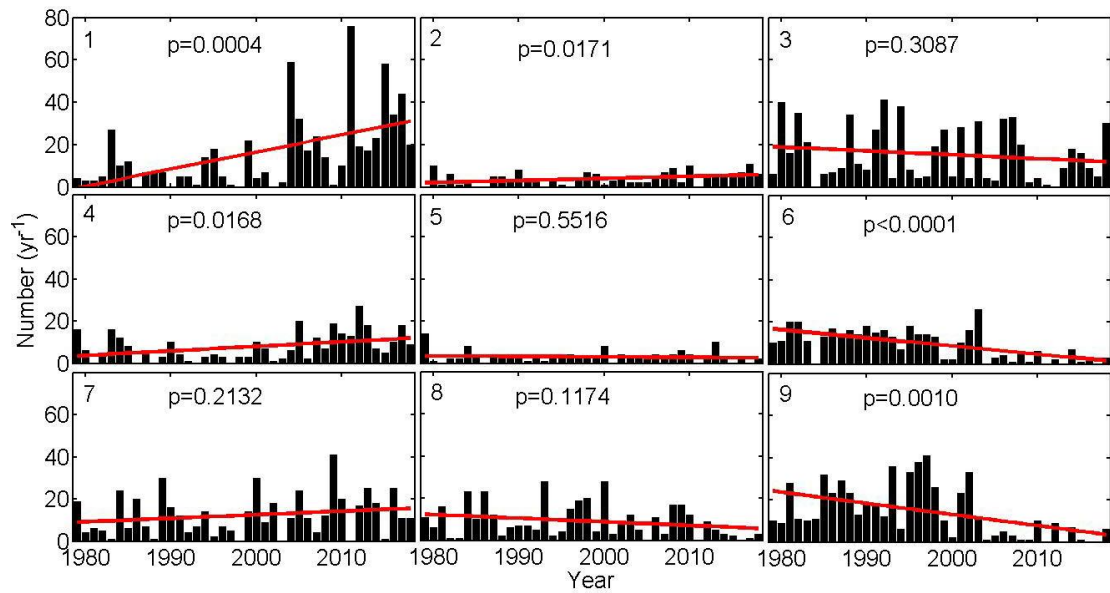
1166
1167
1168
1169
1170
1171
1172
1173
1174
1175
1176
1177



1178
1179
1180
1181
1182

Figure 6. Corresponding anomalous wintertime sea ice concentration without removing its linear trend from the NSIDC over the 1979-2019 period for each node in Figure 1. Dotted regions indicate the above 95% confidence level.

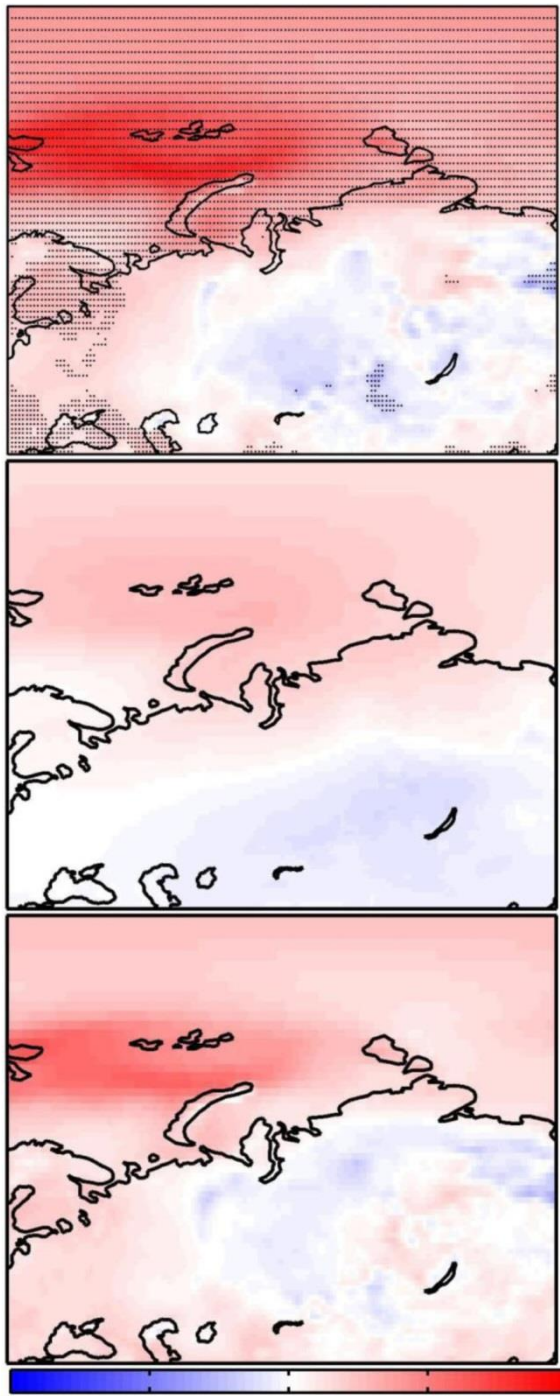
1183
1184
1185
1186
1187
1188
1189
1190
1191
1192
1193
1194
1195
1196
1197



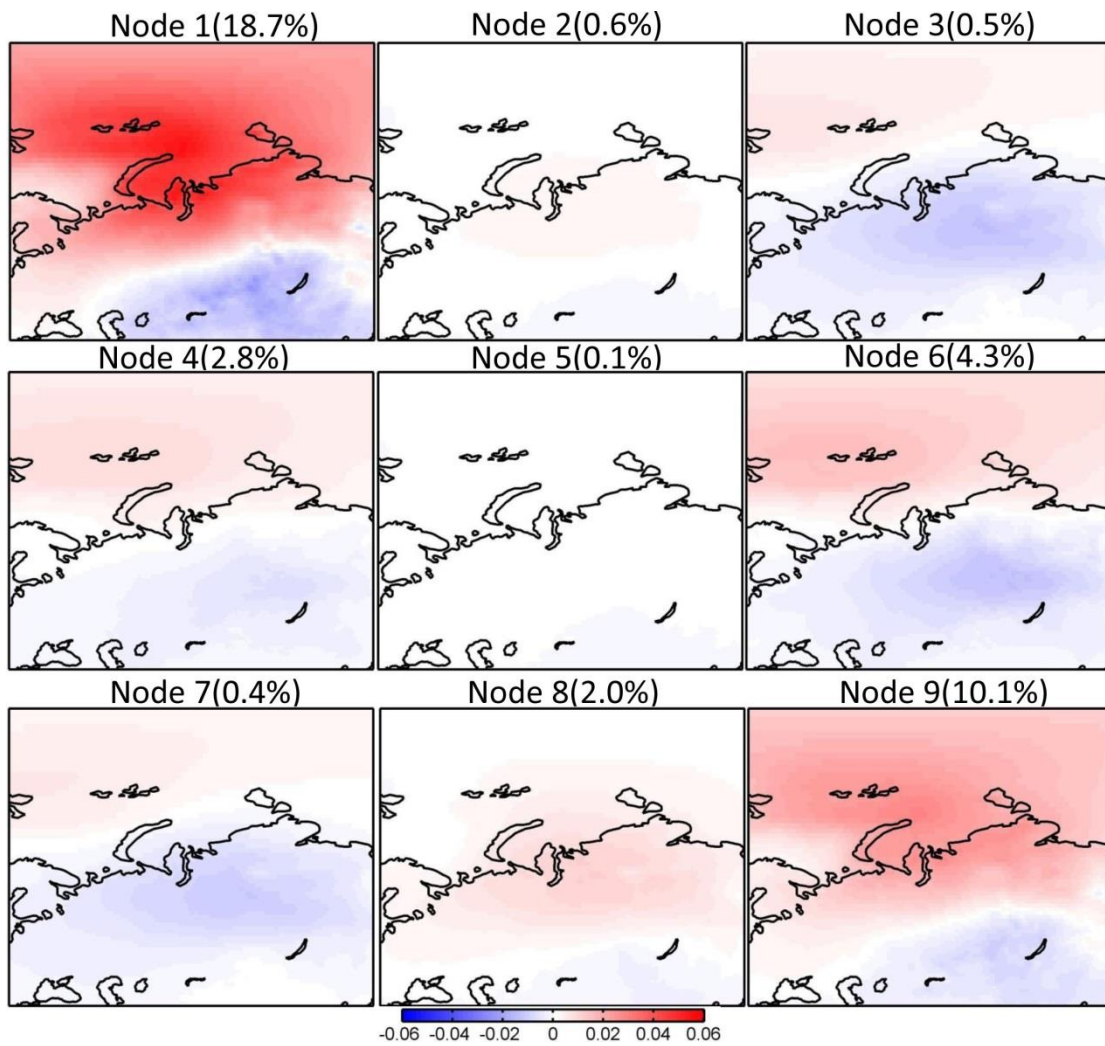
1198
1199
1200
1201
1202
1203
1204
1205
1206
1207
1208
1209
1210
1211
1212

Figure 7. Time series of the number of days for occurrence of each SOM node in Figure 1 over the 1979-2019 period. The thick lines denote the trend in time series.

1213
1214
1215



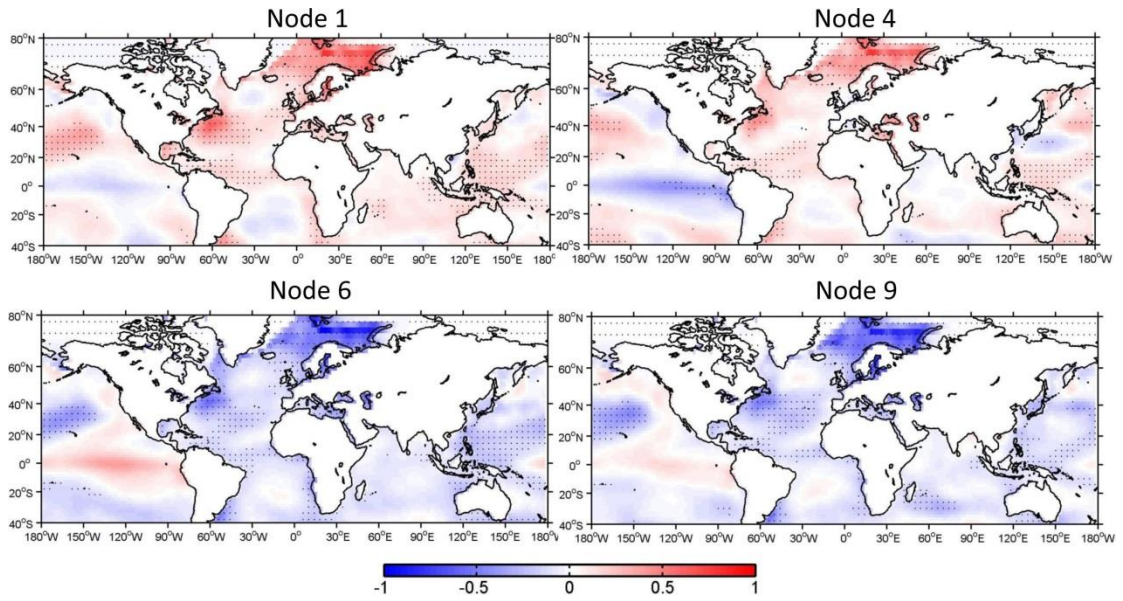
1216 -0.4 -0.2 0 0.2 0.4
1217 Figure 8. Total (top), SOM-explained (middle), and residual (bottom) trend in wintertime (DJF)
1218 surface air temperature ($^{\circ}\text{C yr}^{-1}$) over the 1979-2019 period. Dots in the top panel indicate above
1219 95% confidence level.
1220



1221
 1222
 1223
 1224
 1225
 1226
 1227
 1228
 1229
 1230
 1231
 1232
 1233
 1234
 1235
 1236
 1237
 1238
 1239
 1240

Figure 9. Trends in surface air temperature explained by each SOM node ($^{\circ}\text{C yr}^{-1}$) over the 1979-2019 period. The percentage in the upper of each panel indicates the fraction of the total trend represented by each node.

1241
1242



1243

1244 Figure 10. Anomalous SST (°C) regressed into the normalized time series of occurrence number
1245 for nodes 1, 4, 6, and 9 without removing its linear trend from the NOAA over the 1979-2019
1246 period.

1247

1248

1249

1250

1251

1252

1253

1254

1255

1256

1257

1258

1259

1260

1261

1262

1263

1264

1265

1266

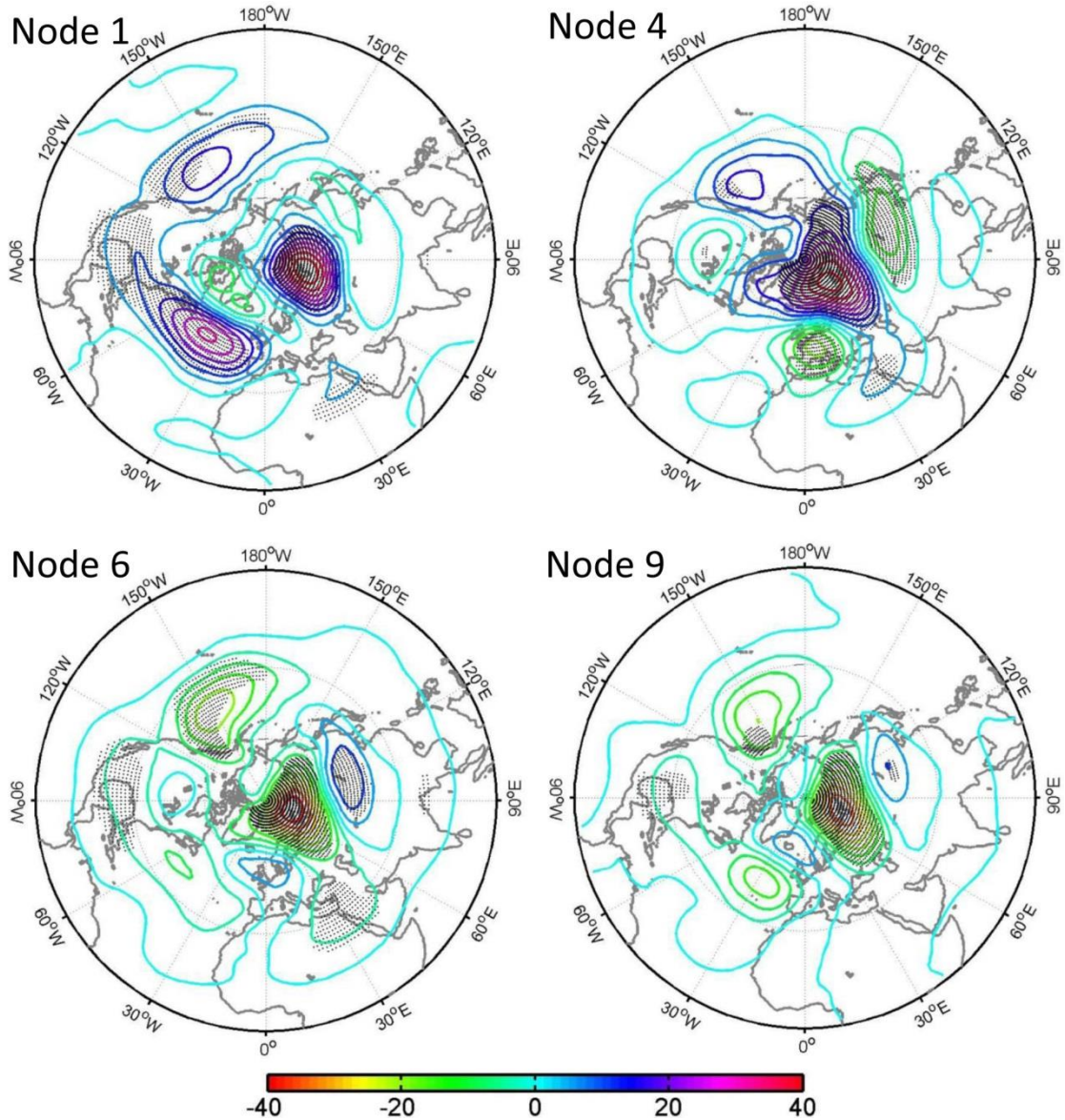
1267

1268

1269

1270

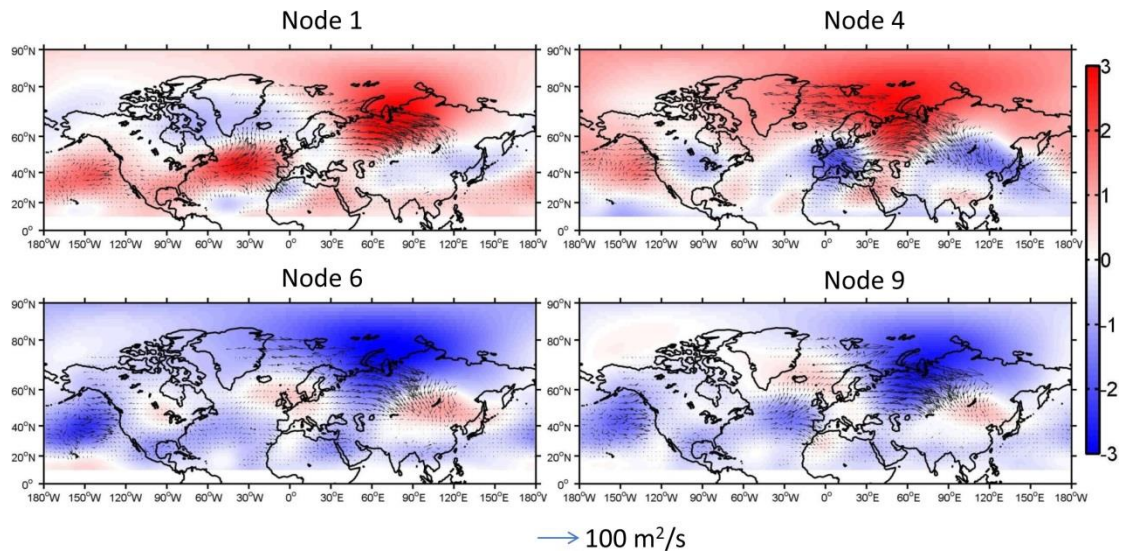
1271
1272
1273
1274



1275
1276
1277
1278
1279
1280
1281
1282
1283
1284
1285
1286

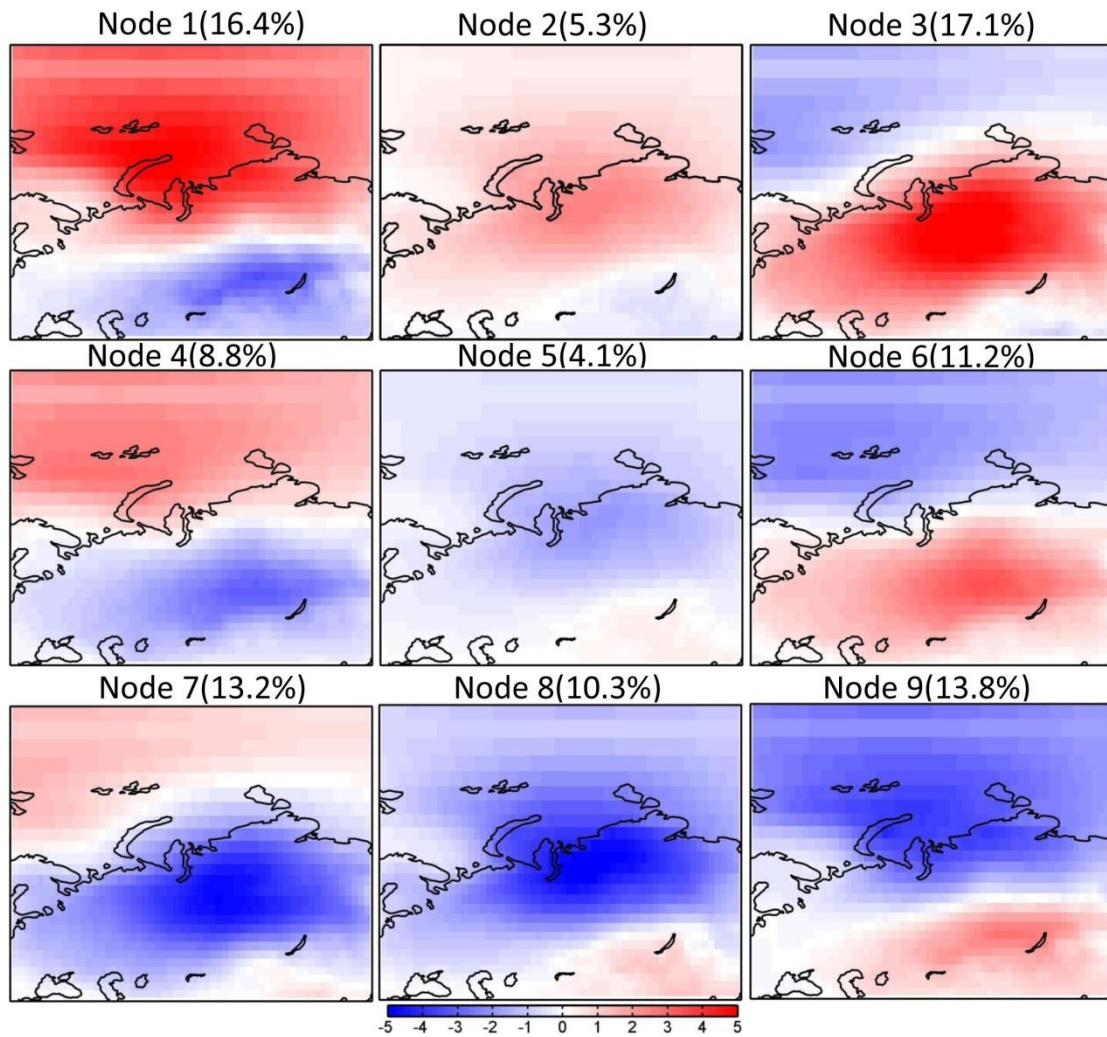
Figure 11. Anomalous 500-hPa geopotential height (gpm) regressed into the normalized time series of occurrence number for nodes 1, 4, 6, and 9 without removing its linear trend from ERA-Interim reanalysis over the 1979-2019 period.

1287
1288
1289
1290
1291



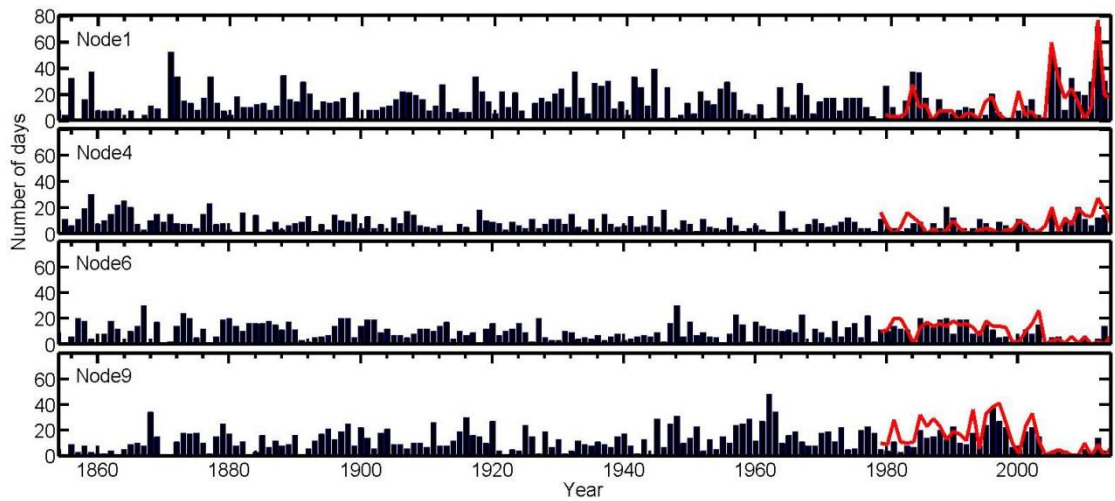
1292
1293
1294
1295
1296
1297
1298
1299
1300
1301
1302
1303
1304
1305

Figure 12. The anomalous wave activity flux (vectors) (Takaya and Nakamura, 2001) and stream function (colors, units: $10^7 \text{ m}^2/\text{s}^{-1}$) regressed onto the normalized time series of occurrence number for nodes 1, 4, 6, and 9 without removing their linear trends from ERA-Interim reanalysis over the 1979-2019 period.



1306
 1307
 1308
 1309
 1310
 1311
 1312
 1313
 1314
 1315
 1316
 1317
 1318
 1319
 1320
 1321
 1322
 1323
 1324
 1325
 1326

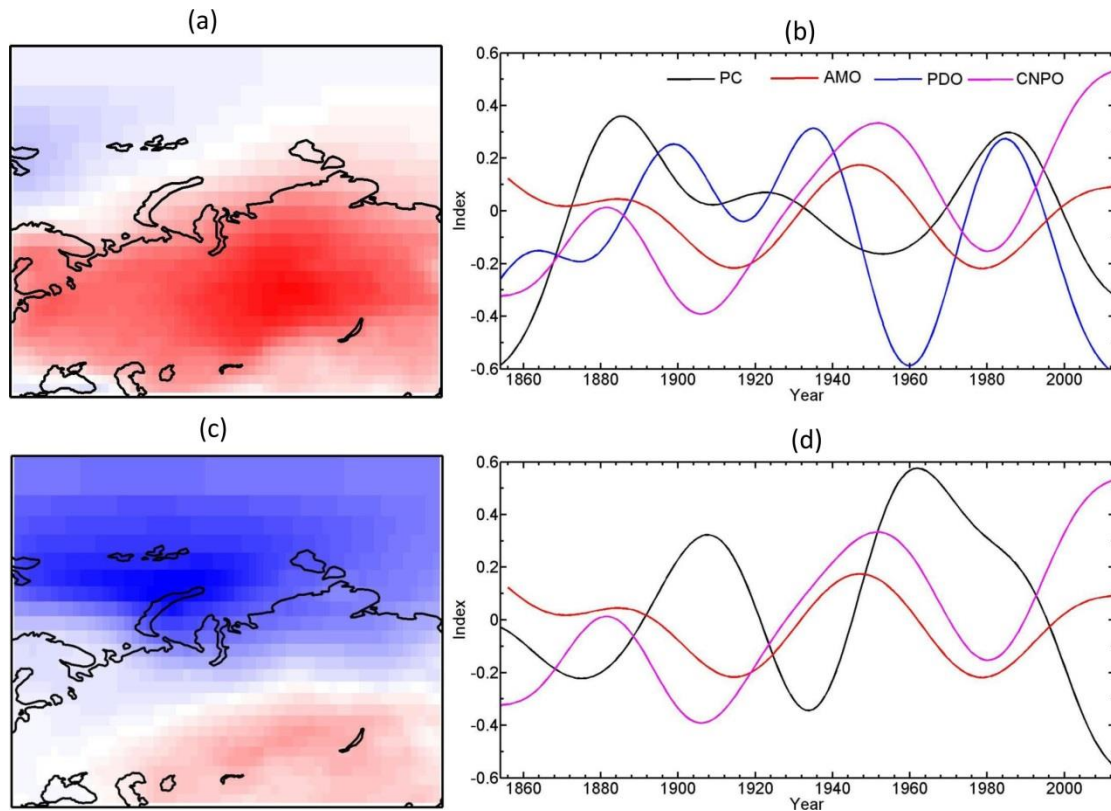
Figure 13. Spatial patterns of SOM nodes for detrended daily wintertime (December, January, and February) surface air temperature anomalies (°C) from the 20CR reanalysis for the 1851-2014 period. The number in brackets denotes the frequency of the occurrence for each node.



1327
 1328
 1329
 1330
 1331
 1332
 1333
 1334
 1335
 1336
 1337
 1338
 1339
 1340
 1341
 1342
 1343
 1344
 1345
 1346
 1347
 1348
 1349
 1350
 1351
 1352
 1353
 1354
 1355
 1356
 1357
 1358
 1359

Figure 14. Time series of the number of days for occurrence of each SOM node in Figure 13 from the 20CR reanalysis for the 1851-2014 period. The thick red lines denote the result in Figure 7 from the ERA-Interim reanalysis for the 1979-2019 period.

1360
1361



1362

1363 Figure 15. The (a) leading pattern and (b) its time series (PC1 and PC2) of EOF analysis of
1364 wintertime surface air temperature anomalies [from the 20CR reanalysis for the 1851-2014 period.](#)
1365 Prior to EOF analysis, surface air temperature data are detrended. A 40-yr low-pass filter is
1366 applied to the time series of PC1, PC2, AMO, PDO, and central North Pacific Ocean (CNPO)
1367 indices. The correlation coefficients between PC1 and AMO, PDO and CNPO indices are -0.46
1368 ($p < 0.0001$), 0.38 ($p < 0.0001$), and -0.19 ($p = 0.019$); those between PC2 and
1369 AMO, PDO and CNPO indices are -0.44 ($p < 0.0001$), 0.38 ($p < 0.0001$), and -0.26 ($p = 0.0009$).

1370